effect of ionizing radiation by brief concomitant exposures to angiostatin. *Cancer Res* 1998; **58**: 5686–9.
7 Mauceri HJ, Hanna NN, Beckett MA *et al.* Combined effects of angiostatin and ionizing radiation in antitumour therapy. *Nature* 1998; **394**: 287–91.
8 Ingber D, Fujita T, Kishimoto S *et al.* Synthetic analogues of fumagillin that inhibit angiogenesis and suppress tumour growth. *Nature (Lond)*, 1990; **348**: 555–7.
9 Zhang Y, Griffith EC, Sage J, Jacks T, Liu JO. Cell cycle inhibition by the anti-angiogenic agent TNP-470 is mediated by p53 and p21WAF1/CIP1. *Proc Natl Acad Sci USA* 2000; **97**: 6427–32.
10 Sin N, Meng L, Wang MQ, Wen JJ, Bommann WG, Crews CM. The anti-angiogenic agent fumagillin covalently binds and inhibits the methionine aminopeptidase, MetAP-2. *Proc Natl Acad Sci USA* 1997; **94**: 6099–103.
11 Yanase T, Tamura M, Fujita K, Kodama S, Tanaka K. Inhibitory effect of angiogenesis inhibitor TNP-470 on tumor growth and metastasis of human cell lines in vitro and in vivo. *Cancer Res* 1993; **53**: 2566–70.
12 Yoshida T, Kaneko Y, Tsukamoto A, Han K, Ichinose M, Kimura S. Suppression of hepatoma growth and angiogenesis by a fumagillin derivative TNP 470. *Cancer Res* 1998; **58**: 3751–6.
13 Miura S, Emoto M, Matsuo Y, Kawarabayashi T, Saku K. Carcinosarcoma-induced endothelial cells tube formation through KDR/Flk-1 is blocked by TNP-470. *Cancer Lett* 2004; **203**: 45–50.
14 Emoto M, Iwasaki H, Kikuchi M *et al.* Two cell lines established from mixed Müllerian tumors of the uterus: Morphological, immunocytochemical, and cytogenetic analyses. *Cancer* 1992; **69**: 1759–68.
15 Lund EL, Bastholm L, Kristjansen PE. Therapeutic synergy of TNP-470 and ionizing radiation: effects on tumor growth, vessel morphology, and angiogenesis in human glioblastoma multiforme xenografts. *Clin Cancer Res* 2000; **6**: 971–8.
16 Saad AH, Hahn GM. Ultrasound enhanced drug toxicity on Chinese hamster ovary cells *in vitro*. *Cancer Res* 1989; **49**: 5931–4.
17 Loverock P, ter Haar G, Ormerod MG, Imrie PR. The effect of ultrasound on the cytotoxicity of adriamycin. *Br J Radiol* 1990; **63**: 542–6.
18 Worthington AE, Thompson J, Rauth AM, Hunt JW. Mechanism of ultrasound enhanced porphyrin cytototoxicity. Part I. A search for free radical effects. *Ultrasound Med Biol* 1993; **19**: 123–5.
19 Tomizawa M, Ebara M, Saisho H, Sakiyama S, Tagawa M. Irradiation with ultrasound of low output intensity increased chemosensitivity of subcutaneous solid tumors to an anti-cancer agent. *Cancer Lett* 2001; **173**: 31–5.
20 Brayman AA, Coppage ML, Vaidya S, Miller MW. Transient poration and cell surface receptor removal from human lymphocytes in vitro by 1 MHz ultrasound. *Ultrasound Med Biol* 1999; **25**: 999–1008.
21 Tachibana K, Uchida T, Ogawa K, Yamashita N, Tamura, K. Induction of cell-membrane porosity by ultrasound. *Lancet* 1999; **353**: 1409.
22 Tachibana K, Uchida T, Hisano S, Morioka E. Eliminating adult T-cell leukaemia cells with ultrasound. *Lancet* 1997; **349**: 325.
23 Tata D, Hahn G, Dunn F. Ultrasonic absorption frequency dependence of two widely used anti-cancer drugs: doxorubicin and daunorubicin. *Ultrasonics* 1993; **31**: 447–50.
24 Misik V, Riesz P. Free radical intermediates in sonodynamic therapy. *Ann NY Acad Sci* 2000; **899**: 335–48.
25 Otsuka T, Ohakawa T, Shibata T *et al.* A new potent angiogenesis inhibitor, FR118487. *J Microbiol Biotechnol* 1991; **1**: 163–8.
26 Emoto M, Iwasaki H, Ishiguro M *et al.* Angiogenesis in carcinosarcomas of the uterus: differences in the microvessel density and expression of vascular endothelial growth factor between the epithelial and mesenchymal elements. *Hum Pathol* 1999; **30**: 1232–41.
27 Kudelka AP, Verschraegen CF, Loyer E. Complete remission of metastatic cervical cancer with the angiogenesis inhibitor TNP-470. *N Eng J Med* 1998; **338**: 991–2.
28 Bhargava P, Marshall JL, Rizvi N *et al.* A phase I and pharmacokinetic study of TNP-470 administered weekly to patients with advanced cancer. *Clin Cancer Res* 1999; **5**: 1989–95.
29 Satchi-Fainaro R, Puder M, Davies JW *et al.* Targeting angiogenesis with a conjugate of HPMA copolymer and TNP-470. *Nat Med* 2004; **10**: 255–61.
30 Ter Haar G. Therapeutic applications of ultrasound. *Prog Biophys Mol Biol* 2007; **93**: 111–29.
31 Longo FW, Longo WE, Tomashefsky P, Lattimer JK, Rivin BD, Tannenbaum M. Interaction of ultrasound with neoplastic tissue. Local effect on subcutaneously implanted Furth-Columbia rat Wilms' tumor. *Urology* 1975; **6**: 631–4.
32 Yang R, Reilly CR, Rescorla FJ *et al.* High-intensity focused ultrasound in the treatment of experimental liver cancer. *Arch Surg* 1991; **126**: 1002–9.
33 Nicolai H, Steinbach P, Knuechel-Clarke R *et al.* Proliferation of tumor spheroids after shock-wave treatment. *J Cancer Res Clin Oncol* 1994; **120**: 438–41.
34 Feril LB Jr, Kondo T, Zhao QL *et al.* Enhancement of ultrasound-induced apoptosis and cell lysis by echo-contrast agents. *Ultrasound Med Biol* 2003; **29**: 331–7.
35 Gee MS, Saunders HM, Lee JC *et al.* Doppler ultrasound imaging detects changes in tumor perfusion during antivascular therapy associated with vascular anatomic alterations. *Cancer Res* 2001; **61**: 2974–82.
36 Abdollahi A, Lipson KE, Sckell A *et al.* Combined therapy with direct and indirect angiogenesis inhibition results in enhanced antiangiogenic and antitumor effects. *Cancer Res* 2003; **63**: 8890–8.
37 Emoto M, Fujimitsu R, Iwasaki H, Kawarabayashi T. Diagnostic challenges in patients with tumors: case 3. A normal-sized ovarian cancer detected by color Doppler ultrasound using a microbubble contrast agent. *J Clin Oncol* 2003; **21**: 3703–5.
38 Chen C-N, Cheng Y-M, Liang J-T *et al.* Color Doppler vascularity index can predict distant metastasis and survival in colon cancer patients. *Cancer Res* 2000; **60**: 2892–7.
39 Emoto M, Charnock-Jones DS, Licence D *et al.* Localisation of the VEGF and angiopoietin genes in uterine carcinosarcoma. *Gynecol Oncol* 2004; **95**: 474–82.

Available online at www.sciencedirect.com
SCIENCE DIRECT
Cancer Letters 246 (2007) 149–156
CANCER Letters
www.elsevier.com/locate/canlet

Identification of genes responsive to low intensity pulsed ultrasound in a human leukemia cell line Molt-4

Yoshiaki Tabuchi [a,*], Hidetaka Ando [c], Ichiro Takasaki [a], Loreto B. Feril Jr [b,e], Qing-Li Zhao [b], Ryohei Ogawa [b], Nobuki Kudo [d], Katsuro Tachibana [e], Takashi Kondo [b]

[a] *Division of Molecular Genetics, Life Science Research Center, University of Toyama, 2630 Sugitani, Toyama 930-0194, Japan*
[b] *Department of Radiological Sciences, Faculty of Medicine, University of Toyama, Toyama 930-0194, Japan*
[c] *First Department of Surgery, Faculty of Medicine, University of Toyama, Toyama 930-0194, Japan*
[d] *Laboratory of Biomedical Instrumentation and Measurement, Graduate School of Information Science and Technology, Hokkaido University, Sapporo 060-0814, Japan*
[e] *Department of Anatomy, Fukuoka University School of Medicine, Fukuoka 814-0180, Japan*

Received 20 December 2005; received in revised form 15 February 2006; accepted 15 February 2006

Abstract

We examined the gene expression of human leukemia Molt-4 cells treated with non-thermal low intensity pulsed ultrasound. Six hours after 0.3 W/cm^2 pulsed ultrasound treatment, apoptosis (24 ± 3.3%, mean ± SD) with minimal cell lysis was observed. Of approximately 16,600 genes analyzed, BCL2-associated athanogene 3 (*BAG3*), DnaJ (Hsp40) homolog, subfamily B, member 1 (*DNAJB1*), heat shock 70 kDa protein 1B (*HSPA1B*), and heat shock 70 kDa protein 6 (*HSPA6*) showed increased levels of expression while isopentenyl-diphosphate delta isomerase (*IDI1*) and 3-hydroxy-3-methylglutaryl–coenzyme A synthase 1 (*HMGCS1*) showed decreased levels in the cells 3 h after the ultrasound treatment. The expression levels of these six genes were confirmed by a real-time quantitative polymerase chain reaction. To our knowledge, this is the first report of DNA microarray analysis of genes that are differentially expressed in response to apoptosis induced by non-thermal low intensity pulsed ultrasound in human leukemia cells. The present results will provide a basis for further understanding of the molecular mechanisms of effects of not only low intensity pulsed ultrasound but also that of mechanical shear stress in the cells.

Keywords: DNA microarray; Gene expression; Low intensity pulsed ultrasound

1. Introduction

In many medical fields, ultrasound (US) has been widely used for diagnosis and therapy. Biophysical actions of US are divided into three modes, thermal, cavitational and non-thermal non-cavitational effects. Cavitation is known to lead to both mechanical shear stress and free radical formation arising from the oscillation and collapse of cavitation bubbles [1–3]. In general, these two effects (mechanical shear stress and free radicals) of cavitation have been inferred to act simultaneously on all of biological materials. It is well known that fairly intense US induces cell killing, cell lysis, loss of viability and loss of clonogenicity [2]. Currently, of particular interest is its ability to induce apoptosis in human leukemia cell lines [4–12]. Different factors that can influence apoptosis were cited. Among them were, sonochemical mechanism [12], cavitation-mediated enhancement of intracellular calcium ion concentration, intracellular free radical

* Corresponding author. Tel.: +81 76 434 7187; fax: +81 76 434 5176.
E-mail address: ytabu@cts.u-toyama.ac.jp (Y. Tabuchi).

0304-3835/$ - see front matter © 2006 Elsevier Ireland Ltd. All rights reserved.
doi:10.1016/j.canlet.2006.02.011

formation due to mitochondrial membrane damage and free radical formation [10,11], and sonomechanical mechanism [9].

It has been indicated that DNA microarrays are one of the most powerful technologies for functional genomics as it can simultaneously analyze the expression levels of many 100s or many 1000s of genes [13,14]. Recently, we applied DNA microarray technologies to analyze gene expression in cellular differentiation [15] and in a variety of biological responses to physical and chemical stresses, such as sodium butyrate [16], bisphenol A [17,18] and hyperthermia [19]. In our previous study, using UniGEMV Ver2.0 human gene expression microarrays to detect approximately 9200 genes, five up-regulated genes and two down-regulated genes were identified in the human lymphoma U937 cells at 6 h after exposure of fairly intense continuous wâves (1 MHz, 4.9 W/cm^2, for 1 min), where not only free radical formation, but also cell lysis and apoptosis were significantly observed [20]. Moreover, under nearly same condition in U937 cells, another microarray system and real-time quantitative polymerase chain reaction (PCR) confirmed up-regulation of heme oxygenase-1 (HO-1) and revealed that HO-1 is the most sensitive gene for US in U937 cells [21]. More recently, following a report by Lagneaux et al. [12], we also reported that non-thermal low intensity pulsed US treatment (1 MHz, 0.3 W/cm^2, 1 min) induced apoptosis in human leukemia cell lines such as U937, Jurkat and Molt-4, and it was revealed that the up-regulation of HO-1 was observed above apoptosis-inducing intensities [9,22]. However, the knowledge of the details of molecular signaling in response to mechanical pressure or pressure waves such as US, particularly low intensity pulsed waves, remains elusive.

In the present study, the gene expression of human leukemia Molt-4 cells treated with low intensity pulsed US were examined by using high-density IntelliGene HS human Expression microarrays to detect approximately 16,600 genes.

2. Materials and methods

2.1. Cell culture

Molt-4 human leukemia cells were obtained from Japanese Cancer Research Resource Bank (Tokyo, Japan). The cells were grown in RPMI 1640 medium (Invitrogen Co., Tokyo, Japan) supplemented with 10% fetal bovine serum (Invitrogen Co.) at 37 °C in humidified air with 5% CO_2.

2.2. US apparatus and intensity measurement

The ultrasonic apparatus (Sonicmaster ES-2, OG Giken Co. Ltd, Okayama, Japan) with a resonant frequency of 1 MHz with 100 Hz pulse repetition frequency (PRF) was used in all the sonication experiments. This device is equipped with a built-in digital timer, intensity regulator, and duty factor (DF) controller. For the sonication procedure, the transducer with a diameter of 5 cm was fixed with a clamp attached to a metal stand to keep the transducer facing directly upward (Fig. 1). We used such near acoustic field produced by the liquid–air interface and did not reduce the standing waves because of the effective occurrence of cavitation.

The spatial-average–temporal-average intensities (ISATA) at 10% DF corresponding to the reading output intensity were measured using an ultrasonic power meter (PM-DT-10E, Ohmic instrument Co., Easton, MD). The peak acoustic amplitude in degassed water was also measured at the distance of 5 cm from the transducer with a calibrated poly-(vinyledene difluoride–trifluoroethylene) needle-type hydrophone, 0.5 mm in diameter (Toray techno Co., Ltd, Shiga, Japan) connected to a PC/AT compatible computer and a digitizing oscilloscope (TDS3034, Tektronix Japan, Ltd, Tokyo, Japan). The ISATA and the peak acoustic pressures corresponding to the reading output of 0.1, 0.2, 0.3, 0.4 and 0.5 W/cm^2 (device-indicated) were 0.048, 0.072, 0.081, 0.092 and 0.105 W/cm^2, and 0.061, 0.105, 0.132, 0.144 and 0.146 MPa, respectively. In this paper we used device-indicated intensities to refer to these values.

For most of the experiments, 0.3 W/cm^2 was used. During such an ultrasonic exposure experiment the change in absorbance of 2 ml of aqueous air-saturated ferrous (Fricke) dosimeter solution after 5 min exposure at 304 nm was 0.0082 ± 0.0015 (mean $\pm$ SD, $n=4$) in a 1 cm path length quartz cell. This dosimeter monitors the extent of the cavitational activity induced by ultrasound by measuring the sum of H_2O_2, OH radicals, and H atoms available to react with ferrous ions.

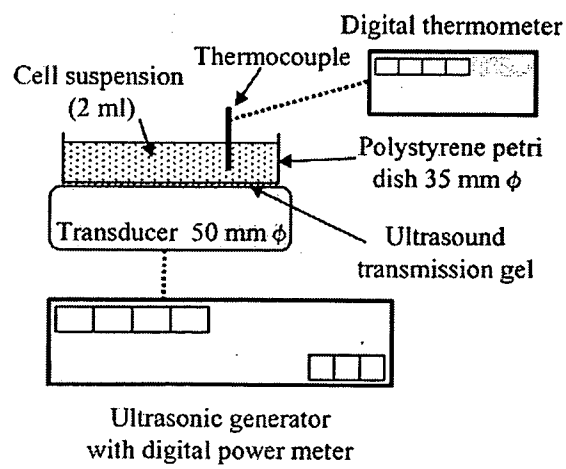

Fig. 1. A set-up for ultrasonic exposure.

2.3. Sonication procedure

The cell concentration used in the experiments was about 2.0×10^6 cells/ml. The cells were gently mixed to homogenize and 1 ml/sample of cell suspension was transferred to a 3 cm polyethylene culture dish. Just before sonication, 1 ml culture medium was added to the cell suspension after gentle shaking. After sonication, the cells were incubated in humidified air with 5% CO_2 at 37 °C for an indicated period before evaluation of DNA fragmentation and other parameters.

2.4. Measurement of cell viability

Trypan blue dye exclusion test was performed. In short, cell suspension was mixed with an equal amount of 0.3% Trypan blue solution (Sigma–Aldrich Co., St Louis, MO) in phosphate-buffered saline. After 5 min incubation at room temperature, the number of cells excluding Trypan blue (unstained) was counted using a Burker Turk hemocytometer to estimate the number of intact viable cells and the number of non-viable cells.

2.5. DNA fragmentation assay

The amount of DNA extracted from cells that had undergone DNA fragmentation was assayed using the method of Sellins and Cohen [23] with a few modifications. Briefly, cells were lysed in lysis buffer (1 mM EDTA, 0.2% Triton X-100 and 10 mM Tris–HCl, pH 7.5) and centrifuged at 13,000 g for 10 min. Subsequently, each DNA sample in the supernatant and the resulting pellet were precipitated in 12.5% trichloroacetic acid (TCA) at 4 °C, and quantified using the diphenylamine reagent after hydrolysis in 5% TCA at 90 °C for 20 min. The percentage of fragmented DNA for each sample was calculated as the amount of DNA in the supernatant divided by the total DNA for that sample (supernatant plus pellet).

2.6. Electron paramagnetic resonance (EPR)-spin trapping for the detection of free radical formation

In this study, we used EPR-spin trapping with 5,5-dimethyl-1-pyrroline-*N*-oxide (DMPO) to detect the US-induced hydroxyl radical formation [2,24]. The cells suspended in culture medium with 10 mM of DMPO were sonicated at 0–0.5 W/cm^2 of 1 MHz 10% DF for 1 min. At 9.425 GHz with a field modulation of 0.1 mT amplitude using a microwave power of 4 mW, EPR spectra of the sonicated solution in a capillary tube were recorded with EPR spectrometer (RFR-30, Radical Research Inc., Tokyo, Japan) at room temperature. The yields of spin adducts were determined using a stable nitroxide radical, TEMPOL (4-hydroxy-2,2,6,6-tetramethyl-1-piperidinyloxy) as a standard. A calibration curve was determined by plotting the product of the peak-to-peak derivative amplitude and the square of the width at maximum slope of the signal versus the different concentrations of the standard nitroxide radical. One unit of the *Y*-axis labeled 'DMPO-OH adduct' is calculated to correspond to about 19.0 μM of TEMPOL.

2.7. Separation of total RNA and mRNA

Total RNA was extracted from the cells using an RNeasy Total RNA Extraction Kit (Qiagen K.K., Tokyo, Japan). Then, RNA samples were treated with RNase-free DNase (Qiagen K.K.) for 30 min at room temperature. mRNAs were extracted from the DNase-treated samples using an Oligotex-dT30 mRNA Purification Kit (Takara Bio Inc., Shiga, Japan).

2.8. cDNA microarray analysis

cDNA microarray analysis was performed by IntelliGene HS human Expression glass microarrays (Takara Bio Inc.), which were spotted with approximately 16,600 cDNA fragments of human genes. A list of these genes is available at Takara's Web site (http://www.takara-bio.co.jp/). Antisense RNA (aRNA) labeled with Cy3 (control group) or Cy5 (treated group) from mRNAs from cells at 3 h after US treatment (for 1 min at 0.3 W/cm^2) by using an RNA Transcript SureLABEL Core Kit (Takara Bio Inc.). In some experiments, control sample was labeled with Cy5; and in others, it was labeled with Cy3, with essentially identical results. Hybridization and washing of the microarray were carried out according to the manufacturer's instructions. In brief, aRNA probe solutions containing both Cy3- and Cy5-labeled aRNA probes were applied to the microarrays, and the microarrays were covered with a spaced glass cover slip (Takara Bio Inc.) and placed in a humidified chamber at 70 °C for 16 h with gentle shaking. Then, the microarrays were sequentially washed in 2× SSC (150 mM NaCl and 15 mM sodium citrate) containing 0.2% SDS for 10 min three times at 65 °C and in 0.05× SSC for 1 min once at room temperature. The microarrays were scanned in both Cy3 and Cy5 channels with a ScanArray Lite (Packard BioChip Technologies, Billerica, MA, USA). QuantArray software (Packard BioChip Technologies) was used for image analysis. Genes were considered to be positive-expressed if the signal/background ratio was >2.0. The average of RPS27A (ribosomal protein S27a, an internal control gene) Cy3 and Cy5 signal (12 spots each) gives a ratio that was used to balance or normalize the signals.

2.9. Real-time quantitative PCR assay

Real-time quantitative PCR was performed on a Real-Time PCR system (Mx3000P, Stratagene Japan K.K., Tokyo, Japan) using Brilliant SYBR Green qPCR Master Mix (Stratagene Japan K.K.) according to the manufacturer's protocol. Reverse transcriptase reaction (Omniscript Reverse Transcriptase, Qiagen K.K.) was carried out with DNase-treated total RNA by using an oligo d(T)$_6$ primer. Real-time

Table 1
Nucleotide sequences of primers for target genes

Genes	Orientation	Nucleotide sequence (position)	GenBank accession no.
HSPA1B	Sense	5′-AGGTGCAGGTGAGCTACAAG-3′ (509–528)	NM_005346
	Antisense	5′-ATGATCCGCAGCACGTTGAG-3′ (722–703)	
BAG3	Sense	5′-CGACCAGGCTACATTCCCAT-3′ (574–593)	NM_004281
	Antisense	5′-TCTGGCTGAGTGGTTTCTGG-3′ (749–730)	
HSPA6	Sense	5′-GGCCATGACCAAGGACAACA-3′ (1760–1779)	NM_002155
	Antisense	5′-AACCATCCTCTCCACCTCCT-3′ (1976–1957)	
DNAJB1	Sense	5′-ACCCGGACAAGAACAAGGAG-3′ (135–154)	NM_006145
	Antisense	5′-GCCACCGAAGAACTCAGCAA-3′ (364–345)	
IDI1	Sense	5′-CACTAACCACCTCGACAAGC-3′ (304–323)	NM_004508
	Antisense	5′-CTTCTTGGTCTCAGCTCC-3′ (400–383)	
HMGCS1	Sense	5′-ACGGTATGCCCTGGTAGTTG-3′ (564–583)	NM_002130
	Antisense	5′-GCGGTCTAATGCACTGAGGT-3′ (807–788)	
RPS27A	Sense	5′-TTACGGGGAAGACCATCACC-3′ (61–80)	NM_002954
	Antisense	5′-CCACCACGAAGTCTCAACAC-3′ (265–246)	

BAG3, BCL2-associated athanogene 3; *DNAJB1*, DnaJ (Hsp40) homolog, subfmaily B, member 1; *HMGCS1*, 3-hydroxy-3-methylglutaryl–coenzyme A synthase 1; *HSPA1B*, heat shock 70 kDa protein 1B; *HSPA6*, heat shock 70 kDa protein 6; *IDI1*, isopentenyl-diphosphate delta isomerase; *RPS27A*, ribosomal protein S27a

quantitative PCR was performed by using the specific primers listed in Table 1. Temperature cycling conditions for each primer consisted of 10 min at 95 °C followed by 40 cycles for 30 s at 95 °C, 1 min at 60 °C and 1 min at 72 °C. The dissociation analysis was carried out over the range from 55 to 95 °C by monitoring SYBR Green fluorescence and PCR-specific products were determined as a single peak at the melting curves more than 80 °C. In addition, the specificity of primers was confirmed as a single band with the correctly amplified fragment size through an agarose gel electrophoresis of the real-time quantitative PCR products. Each mRNA expression level was normalized with respect to the mRNA expression of RPS27A.

2.10. Statistical analysis

Data are presented as means ± SD. Statistical analysis was carried out using Student's *t*-test and *P* values less than 0.05 were regarded as significant.

3. Results

3.1. Effects of ultrasonic intensity on cell viability and apoptosis in human leukemia Molt-4 cells

As shown in Fig. 2(A), the cell viability detected by trypan blue dye exclusion test 6 h after the low intensity pulsed US treatment (1 min) was significantly decreased at intensities more than 0.2 W/cm^2, with the cell viability of 88.4 ± 9.3 (%), 79.8 ± 8.5 and 44.2 ± 6.2 at intensities of 0.3, 0.4 and 0.5 W/cm^2, respectively. On the other hand, the apoptosis detected by observing the DNA fragmentation assay 6 h after the low intensity pulsed US treatment (1 min) was significantly increased at intensities more than 0.2 W/cm^2, 24.0 ± 3.3 (%), 26.0 ± 4.6, and 26.5 ± 2.4 at intensities of 0.3, 0.4 and 0.5 W/cm^2, respectively (Fig. 2(B)). Next, the relationship between ultrasonic intensity and free radical formation was studied using EPR-spin trapping with DMPO. The EPR signal of DMPO-OH adducts 1 min after the low intensity pulsed US treatment (1 min) was not detected up to 0.2 W/cm^2, and increased with increasing intensity up to 0.5 W/cm^2. The values of intensities of 0.3, 0.4 and 0.5 W/cm^2 were 0.015 ± 0.01 (relative units), 0.044 ± 0.023 and 0.059 ± 0.022, respectively (Fig. 2(C)). During the sonication procedure, low intensity pulsed US at 0.3 W/cm^2 for 1 min slightly increased the temperature of medium 0.30 ± 0.10 °C as measure by a digital thermometer (model 7563, Yokogawa Electric Co., Tokyo, Japan). Thus, we considered that thermal effect could be neglected in this US condition. Considering the effects of US on the basis of these data, we chose intensity of 0.3 W/cm^2 for the remainder of our studies.

3.2. Identification of genes responsive to low intensity pulsed ultrasound

To identify genes responsive to non-thermal low intensity pulsed US in the cells, we carried out DNA microarray analysis of cells cultured at 3 h after US treatment (for 1 min at 0.3 W/cm^2). Genes were considered up- or down-regulated, if each value and the average fold change were 1.5 or greater in two different experiments. Of approximately 16,600 genes

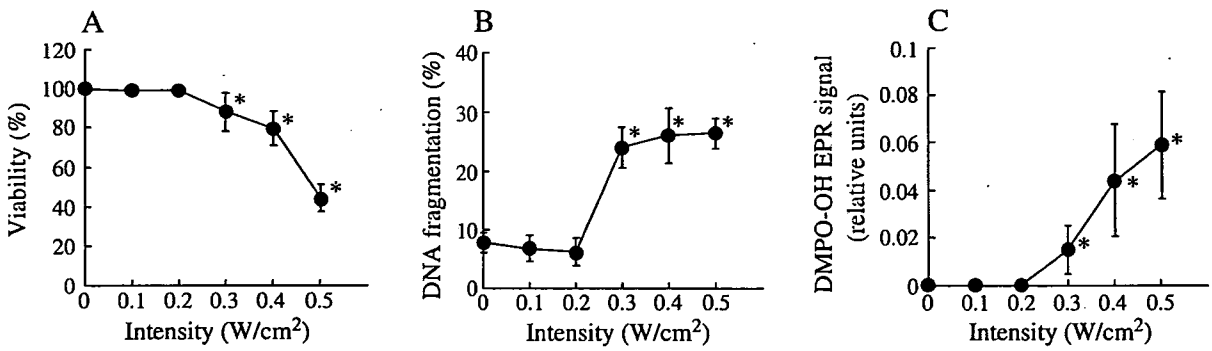

Fig. 2. The effects of ultrasonic intensity on cell viability (A), DNA fragmentation (B) and free radical formation induced by US (C). The cells were sonicated for 1 min at 0–0.5 W/cm^2, 1 MHz pulsed (10% DF, 100 Hz) and cultured at 37 °C. (A) After 6 h culture, the cell viability was evaluated by trypan blue dye exclusion test. (B) After 6 h culture, DNA fragmentation was assayed. (C) After 1 min culture, EPR-spin trapping with DMPO was employed to detect US generated free radicals. One unit of the *Y*-axis is calculated to correspond to about 19.0 μM of TEMPOL. Data indicate means ± SD for four different experiments. *$P < 0.05$ vs. control (intensity: 0 W/cm^2) (Student's *t*-test).

examined, four up-regulated genes, BCL2-associated athanogene 3 (*BAG3*), DnaJ (Hsp40) homolog, subfamily B, member 1 (*DNAJB1*), heat shock 70 kDa protein 1B (*HSPA1B*), and heat shock 70 kDa protein 6 (*HSPA6*), and two down-regulated genes, isopentenyl-diphosphate delta isomerase 1 (*IDI1*) and 3-hydroxy-3-methylglutaryl–coenzyme A synthase 1 (*HMGCS1*) were identified (Table 2). To verify the results of the microarray experiments, real-time quantitative PCR was performed. The results are summarized in Fig. 3. Although the expression levels of these genes were not completely comparable to that found by microarray analysis, the expression levels of *BAG3*, *DNAJB1*, *HSPA1B* and *HSPA6* were significantly increased, with expression levels being 6.3-, 3.3-, 7.3- and 311-fold, respectively. In contrast, the expression levels of *IDI1* and *HMGCS1* were significantly decreased, with the expression levels being 0.45 and 0.34-fold, respectively.

4. Discussion

US have been widely used for diagnosis and therapy in many medical fields. More recently, following a report by Lagneaux et al. [12], we also reported that non-thermal low intensity pulsed US treatment (1 MHz, 0.3 W/cm^2, 1 min) induced apoptosis in human leukemia cell lines such as U937, Jurkat and Molt-4 [9,22]. In addition, low intensity pulsed US have been shown to promote cell proliferation in human skin fibroblasts [25] and to stimulate cell proliferation and differentiation in human periosteal cells [26]. In the present study, non-thermal low intensity pulsed US induced apoptosis with minimal cell lysis and free radical formation was observed in human leukemia Molt-4 cells in the cases of our previous studies [9,22]. In addition, DNA microarray and real-time quantitative PCR analyses suggested that six genes showed changed levels of expression in US-treated Molt-4 cells. To our best knowledge, this is the first report of DNA microarray analysis of genes that are differentially expressed in response to apoptosis induced by non-thermal low intensity pulsed US in human leukemia cells. Of the approximately 16,600 genes analyzed, four genes including *BAG3*, *DNAJB1*, *HSPA1B* and *HSPA6* showed increased levels of expression while two genes including *IDI1* and *HMGCS1* showed decreased levels in Molt-4 cells 3 h after the US treatment. Of the four up-regulated genes, three heat shock proteins (HSPs), HSPA1B, HSPA6 and DNAJB1, were involved. HSPs are important modifying factors in cellular responses to a variety of physiological relevant conditions such as hyperthermia, oxidative stress, exercise and so on, and play important physiological roles for both normal cellular functions and survival after a stress [27]. HSPA1B and HSPA6 or DNAJB1 are isoforms of inducible Hsp70 or Hsp40, respectively. Inducible

Table 2
Up- and down-regulated genes after sonication in Molt-4 cells

Gene	Fold change			Genbank accession no.
	Exp. 1	Exp. 2	Average	
Up-regulated				
HSPA1B	1.9	1.5	1.7	NM_005346
BAG3	1.5	2.1	1.8	NM_004281
HSPA6	1.7	2.6	2.1	NM_002155
DNAJB1	2.2	2.9	2.6	NM_006145
Down-regulated				
IDI1	0.58	0.67	0.62	NM_004508
HMGCS1	0.52	0.66	0.59	NM_002130

Microarray analysis was performed. Details of experimental conditions described in Section 2.

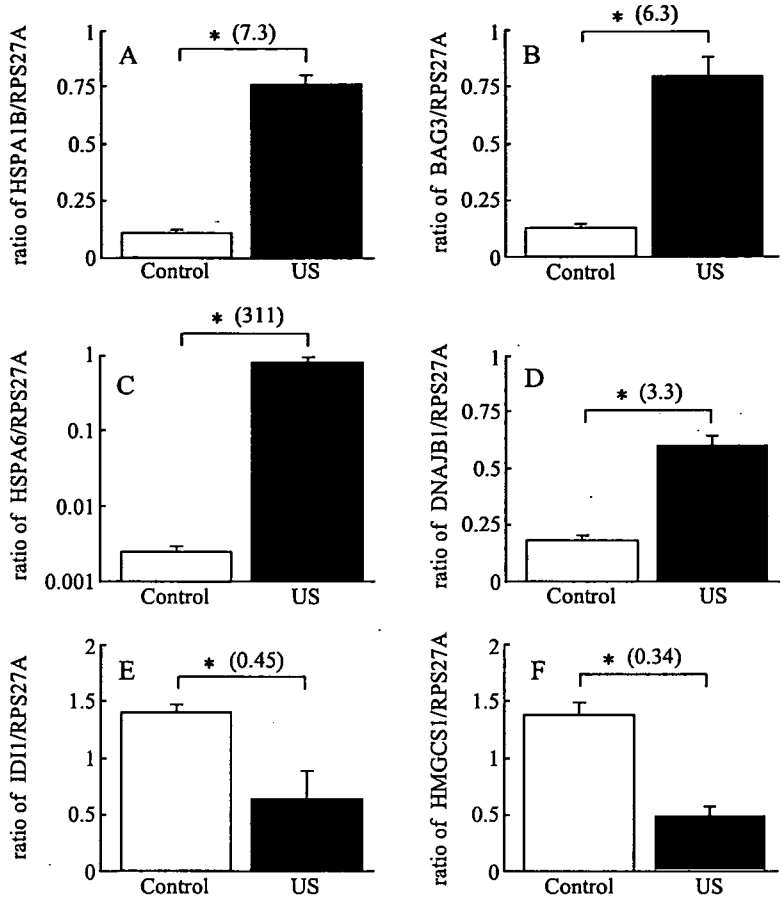

Fig. 3. Verification of the DNA microarray results with real-time quantitative PCR. The cells were exposed to US for 1 min at 0.3 W/cm^2, 1 MHz pulsed (10% DF, 100 Hz) and cultured for 3 h at 37 °C. Reverse transcriptase reaction was carried out with total RNA. Real-time quantitative PCR was performed according to the manufacture's instructions. mRNA level was normalized by *RPS27A*. A, *HSPA1B*; B, *BAG3*; C, *HSPA6*; D, *DNAJB1*; E, *IDI1* and F, *HMGCS1*. Data indicate means ± SD for four different experiments. $*P<0.05$ vs. control (Student's *t* test).

Hsp70 and Hsp40 have been shown to protect cells from necrosis [28] and apoptosis [29,30] and co-operate with Hsp70 [31], respectively. It has been demonstrated that the anti-apoptotic activities of BAG-family proteins including BAG3 may be dependent on their interactions with Hsp70 and/or binding to Bcl-2, an anti-apoptotic protein [32,33]. Interestingly, in the present study, the expression of *BAG3* was significantly elevated in US-treated cells. We therefore speculate that *BAG3* and *Hsps*, *DNAJB1*, *HSPA1B* and *HSPA6*, may be up-regulated to protect cells from apoptosis. IntelliGene HS human Expression microarray used here is spotted with genes for 42 HSPs containing 11 Hsp70 and 21 Hsp40 proteins and four BAG-family proteins. However, only four genes out of 46 genes were increased in this experiment. The mechanisms by which low intensity pulsed US up-regulates these four genes and their physiological roles in US-treated cells remain a subject of further study.

In the present study, genes including IDI1 and HMGCS1 showed decreased levels of expression in the cells treated with US. Both HMGCS1 and IDI1 are enzymes in cholesterol biosynthesis, and the former drives the condensation of acetyl-CoA with acetoacetyl-CoA to form HMG-CoA and the latter catalyzes the rearrangement of isopentenyl diphosphate to its highly electrophilic isomer, dimethylallyl diphosphate [34,35]. It seems likely that the cholesterol biosynthesis pathway is down-regulated in apoptotic cells induced by US. Further studies will be necessary to clarify functions of these two genes in the apoptotic cells induced by low intensity pulsed US.

By using UniGEMV Ver2.0 human gene expression DNA microarrays to detect approximately 9200 genes, we previously demonstrated that five up-regulated genes (ferritin, heavy polypeptide 1, AU RNA-binding protein/enoyl–Coenzyme A hydratase, v-jun avian sarcoma virus 17 oncogene homolog, expressed

sequence tag (GenBank Accession number: N35555) and HO-1) and two down-regulated genes (v-myb avian myeloblastosis viral oncogene homolog and cathepsin G) were identified in the human lymphoma U937 cells at 6 h after exposure to fairly intense continuous waves (1 MHz, 4.9 W/cm^2, for 1 min) which induced significant cell lysis and free radicals [20]. Moreover, under nearly experimental condition, DNA microarray analysis indicated that PCTAIRE protein kinase 1 transcript variant 2 and HO-1 were up-regulated while leukemia inhibitory factor and chemokine ligand 10 were down-regulated by using IntelliGene II Human CHIP 1 DNA microarrays to detect approximately 3900 genes [21]. These microarray and real-time quantitative PCR results suggested that HO-1 is the most sensitive gene in U937 cells treated with low intensity continuous US [20,21]. However, all of these differentially expressed genes containing HO-1 were not identified in our present experiments using low intensity pulsed US. This discrepancy may be due to different experimental conditions such as the type of microarray, intensity of US and origin of the cell.

In conclusion, the present results will provide a basis for further understanding of the molecular mechanisms of biological effects of low intensity pulsed US. Here, we used the standing wave field induced by millisecond pulsed-ultrasound, and the detection of change of gene expression in the progressive wave field remains for further experiment.

Acknowledgements

The authors express their appreciation to Drs Shinichiro Umemura and Hideki Yoshikawa, Central Research Laboratory, Hitachi Co. Ltd, Tokyo, Japan for their support on measurement of peak pressure amplitude of the ultrasonic apparatus. This study is supported in part by the Grant in Aid for Scientific Research on Priority Areas (12217049) from the Ministry of Education, Culture, Sports, Sciences and Technology; in part by the 21st Century COE Program of the Toyama Medical and Pharmaceutical University, Japan; and also in part by Research and Development Committee Program of the Japan Society of Ultrasonics in Medicine.

References

[1] K.S. Suslick, Sonochemistry, Science 247 (1990) 1439–1445.
[2] P. Riesz, T. Kondo, Free radical formation induced by ultrasound and its biological implications, Free Radic. Biol. Med. 13 (1992) 247–270.
[3] L.B. Feril Jr., T. Kondo, Biological effects of low intensity ultrasound: the mechanism involved, and its implications on therapy and on biosafety of ultrasound, J. Radiat. Res. 45 (2004) 479–489.
[4] A. Abdollahi, S. Domhan, J.W. Jenne, M. Hallaj, G. Dell'Aqua, M. Mueckenthaler, et al., Apoptosis signals in lymphoblasts induced by focused ultrasound, Fed. Am. Soc. Exp. Biol. J. 18 (2004) 1413–1414.
[5] H. Ashush, L.A. Rozenszajn, M. Blass, M. Barda-Saad, D. Azimov, J. Radnay, et al., Apoptosis induction of human myeloid leukemic cells by ultrasound exposure, Cancer Res. 60 (2000) 1014–1020.
[6] L.B. Feril Jr., T. Kondo, Major factors involved in the inhibition of ultrasound-induced free radical production and cell killing by pre-sonication incubation or by high cell density, Ultrason. Sonochem. 12 (2005) 353–357.
[7] L.B. Feril Jr., T. Kondo, Q.L. Zhao, R. Ogawa, K. Tachibana, N. Kudo, et al., Enhancement of ultrasound-induced apoptosis and cell lysis by echo-contrast agents, Ultrasound Med. Biol. (2003) 331–337.
[8] L.B. Feril Jr., T. Kondo, K. Takaya, P. Riesz, Enhanced ultrasound-induced apoptosis and cell lysis by a hypotonic medium, Int. J. Radiat. Biol. 80 (2004) 165–175.
[9] L.B. Feril Jr., T. Kondo, Z.G. Cui, Y. Tabuchi, Q.L. Zhao, H. Ando, et al., Apoptosis induced by the sonomechanical effects of low intensity pulsed ultrasound in a human leukemia cell line, Cancer Lett. 221 (2005) 145–152.
[10] H. Honda, Q.L. Zhao, T. Kondo, Effects of dissolved gases and an echo contrast agent on apoptosis induced by ultrasound and its mechanism via the mitochondria-caspase pathway, Ultrasound Med. Biol. 28 (2002) 673–682.
[11] H. Honda, T. Kondo, Q.L. Zhao, L.B. Feril Jr., H. Kitagawa, Role of intracellular calcium ions and reactive oxygen species in apoptosis induced by ultrasound, Ultrasound Med. Biol. 30 (2004) 683–692.
[12] L. Lagneaux, E.C. de Meulenaer, A. Delforge, M. Dejeneffe, M. Massy, C. Moerman, et al., Ultrasonic low-energy treatment: a novel approach to induce apoptosis in human leukemic cells, Exp Hematol. 30 (2002) 1293–1301.
[13] A. Butte, The use and analysis of microarray data, Nat. Rev. Drug Discov. 1 (2002) 951–960.
[14] J. DeRisi, L. Penland, P.O. Brown, M.L. Bittner, P.S. Meltzer, M. Ray, et al., Use of a cDNA microarray to analyse gene expression patterns in human cancer, Nat. Genet. 14 (1996) 457–460.
[15] Y. Tabuchi, T. Kondo, M. Suzuki, M. Obinata, Genes involved in nonpermissive temperature-induced cell differentiation in Sertoli TTE3 cells bearing temperature-sensitive simian virus 40 large T-antigen, Biochem. Biophys. Res. Commun. 329 (2005) 947–956.
[16] Y. Tabuchi, Y. Arai, T. Kondo, N. Takeguchi, S. Asano, Identification of genes responsive to sodium butyrate in colonic epithelial cells, Biochem. Biophys. Res. Commun. 293 (2002) 1287–1294.
[17] Y. Tabuchi, T. Kondo, cDNA microarray analysis reveals chop-10 plays a key role in Sertoli cell injury induced by bisphenol A, Biochem. Biophys. Res. Commun. 305 (2003) 54–61.
[18] Y. Tabuchi, Q.L. Zhao, T. Kondo, DNA microarray analysis of differentially expressed genes responsive to bisphenol A, an alkylphenol derivative, in an in vitro mouse Sertoli cell model, Jpn. J. Pharmacol. 89 (2002) 413–416.

[19] H. Hirano, Y. Tabuchi, T. Kondo, Q.L. Zhao, R. Ogawa, Z.G. Cui, et al., Analysis of gene expression in apoptosis of human lymphoma U937 cells induced by heat shock and the effects of alpha-phenyl *N-tert*-butylnitrone (PBN) and its derivatives, Apoptosis 10 (2005) 331–340.

[20] Y. Tabuchi, T. Kondo, R. Ogawa, H. Mori, DNA microarray analyses of genes elicited by ultrasound in human U937 cells, Biochem. Biophys. Res. Commun. 290 (2002) 498–503.

[21] G. Kagiya, Y. Tabuchi, L.B. Feril, Jr., R. Ogawa, Q.L. Zhao, N. Kudo, et al., Confirmation of enhanced expression of heme oxygenase-1 gene induced by ultrasound and its mechanism: analysis by cDNA microarray system, real-time quantitative PCR, and western blotting, J. Med. Ultrasonics (in press).

[22] H. Ando, L.B. Feril, Jr., T. Kondo, Y. Tabuchi, R. Ogawa, Q.L. Zhao, et al., An echo-contrast agent, Levovist lowers the ultrasound intensity required to induce apoptosis of human leukemia cells, Cancer Lett., in press.

[23] K.S. Sellins, J.J. Cohen, Nuclear changes in the cytotoxic T lymphocyte-induced model of apoptosis, Immunol. Rev. 146 (1995) 241–266.

[24] P. Riesz, T. Kondo, C.M. Krishna, Free radical formation by ultrasound in aqueous solutions. A spin trapping study, Free Radic. Res. Commun. 10 (1990) 27–35.

[25] S. Zhou, A. Schmelz, T. Seufferlein, Y. Li, J. Zhao, M.G. Bachem, Molecular mechanisms of low intensity pulsed ultrasound in human skin fibroblasts, J. Biol. Chem. 279 (2004) 54463–54469.

[26] K.S. Leung, W.H. Cheung, C. Zhang, K.M. Lee, H.K. Lo, Low intensity pulsed ultrasound stimulates osteogenic activity of human periosteal cells, Clin. Orthop. Relat. Res. 418 (2004) 253–259.

[27] K.C. Kregel, Heat shock proteins: modifying factors in physiological stress responses and acquired thermotolerance, J. Appl. Physiol. 92 (2002) 2177–2186.

[28] J.A. Yaglom, D. Ekhterae, V.L. Gabai, M.Y. Sherman, Regulation of necrosis of H9c2 myogenic cells upon transient energy deprivation. Rapid deenergization of mitochondria precedes necrosis and is controlled by reactive oxygen species, stress kinase JNK, HSP72 and ARC, J. Biol. Chem. 278 (2003) 50483–50496.

[29] A. Saleh, S.M. Srinivasula, L. Balkir, P.D. Robbins, E.S. Alnemri, Negative regulation of the Apaf-1 apoptosome by Hsp70, Nat. Cell Biol. 2 (2000) 476–483.

[30] R. Steel, J.P. Doherty, K. Buzzard, N. Clemons, C.J. Hawkins, R.L. Anderson, Hsp72 inhibits apoptosis upstream of the mitochondria and not through interactions with Apaf-1, J. Biol. Chem. 279 (2004) 51490–51499.

[31] R. Kaneko, Y. Hayashi, I. Tohnai, M. Ueda, K. Ohtsuka, Hsp40 a possible indicator for thermotolerance of murine tumour in vivo, Int. J. Hyperthermia 13 (1997) 507–516.

[32] H. Doong, A. Vrailas, E.C. Kohn, What's in the 'BAG'?–A functional domain analysis of the BAG-family proteins, Cancer Lett. 188 (2002) 25–32.

[33] S. Takayama, Z. Xie, J.C. Reed, An evolutionarily conserved family of Hsp70/Hsc70 molecular chaperone regulators, J. Biol. Chem. 274 (1999) 781–786.

[34] F.M. Hahn, J.W. Xuan, A.F. Chambers, C.D. Poulter, Human isopentenyl diphosphate: dimethylallyl diphosphate isomerase: overproduction, purification, and characterization, Arch. Biochem. Biophys. 332 (1996) 30–34.

[35] D.J. Wilkin, S.Y. Kutsunai, P.A. Edwards, Isolation and sequence of the human farnesyl pyrophosphate synthetase cDNA. Coordinate regulation of the mRNAs for farnesyl pyrophosphate synthetase, 3-hydroxy-3-methylglutaryl coenzyme A reductase, and 3-hydroxy-3-methylglutaryl coenzyme A synthase by phorbol ester, J. Biol. Chem. 265 (1990) 4607–4614.

Antitumor effect of TNP-470, an angiogenesis inhibitor, combined with ultrasound irradiation for human uterine sarcoma xenografts evaluated using contrast color Doppler ultrasound

Makoto Emoto,[1,4] Katsuro Tachibana,[2] Hiroshi Iwasaki[3] and Tatsuhiko Kawarabayashi[1]

Departments of [1]Obstetrics and Gynecology, [2]Anatomy, and [3]Pathology, Fukuoka University Medical School, Fukuoka 814-0180, Japan

(Received January 9, 2007/Revised February 8, 2007/Accepted February 21, 2007/Online publication April 6, 2007)

Microvascular endothelial cells, which are recruited by tumors, have become an important target in cancer therapy. This study firstly examined the antitumor effect of angiogenesis inhibitor combined with ultrasound (US) irradiation for human cancer *in vivo* and evaluated its vascularity using color Doppler US in real time with a microbubble US contrast agent. A human uterine sarcoma cell line, FU-MMT-1, was used *in vivo* because this tumor is one of the most malignant neoplasms of the human solid tumors and it also has a poor response to any of the chemotherapeutic agents currently used, as well as to radiotherapy. In angiogenic inhibitors, TNP-470 was selected to use in an *in vivo* study, because this agent showed a higher inhibitory effect in tube formation assay *in vitro*, than that of FR118487, or thalidomide. The FU-MMT-1 xenografts in nude mice were treated using US at a low-intensity (2.0 w/cm², 1MHZ) for 4 min three times per week each after the subcutaneous injection of TNP-470 (30 mg/kg), an angiogenesis inhibitor, and this treatment was continued for 8 weeks. Either treatment of US alone or TNP-470 alone showed a suppression of tumor growth, in comparison to the non-treatment group (control), and a significantly enhanced effect was obtained using the combined treatment. A reduction in the intratumoral vascularity, which was evaluated using both color Doppler and immunohistochemistry, was significantly demonstrated using the combined treatment, in comparison to each treatment alone, and the control. No side-effect was observed in any mice in the combined treatment group. These results suggest that the antitumor effect of TNP-470 for uterine sarcoma was accelerated by US irradiation *in vivo* and this combination might be a potentially effective for new cancer therapy. (*Cancer Sci* 2007; 98: 929–935)

Angiogenesis, the growth of new capillary blood vessels from pre-existing vasculature, is a crucial process for tumor progression and metastasis.[1] The microvascular endothelial cells (EC), which are recruited by tumors, have thus become an important second target in cancer therapy.[2] Angiogenesis inhibitors have thus been developed to target vascular EC and block tumor angiogenesis. Anti-angiogenic therapy alone has been shown to be able to suppress the growth of established tumors and a recent clinical trial showed successful results for advanced rectal cancer.[3] The addition of antiangiogenic agents to chemotherapy,[4,5] radiation,[6,7] or molecular-targeting agents has thus been suggested to potentially increase clinical efficacy. Gorski *et al.* showed that radiotherapy and antibodies against VEGF had a synergistic effect against primary tumors.[6] According to an analysis of a bibliographic database, MEDLINE, however, no previous study has ever examined the combination of angiogenesis inhibitors and ultrasound (US) irradiation in the field of cancer research.

O-(chloroacetyl-carbamoyl)fumagillol (TNP-470) is a low-molecular-weight synthetic analog of fumagillin, a natural compound secreted by the fungus *Aspergillus fumigatus fresenius*.[8] TNP-470 blocks endothelial cell cycle progression in the late G1 phase by activating p53 through a mechanism leading to cyclin-dependent kinase inhibitor $p21^{CIP/WAF}$ expression.[9] The cellular target of TNP-470 was found to be methionine aminopeptidase-2 (MetAP-2), an intracellular enzyme necessary for the process of protein myristolation.[10] The antitumor effect of TNP-470 has been shown in various tumors of human malignancies both *in vitro* and *in vivo*.[11–13] Our previous studies have shown that TNP-470 inhibited the VEGF production and proliferation of a uterine sarcoma cell line, FU-MMT-1, *in vitro*[13] which had been established from a patient with uterine carcinosarcoma.[14] The combination of TNP-470 and cytotoxic agents[4,5] or radiation[15] has showed a successful outcome *in vivo*.

US has been shown to enhance the antitumor effect of a chemotherapeutic agent *in vitro* and *in vivo*.[16–19] Transiently increased permeability of the cell membrane is one of the mechanisms of the US-enhanced chemotherapy.[20] Sonoporation, and resealing of the cell membrane by acoustic pressure are considered to be a primary reason for an increased intracytoplasmic concentration of the administered agent.[21] Ablation of adult T-cell leukemia cells and lysis of HL-60 cells by low-intensity US is enhanced in the presence of a photosensitizing drug, indicating that the photosensitive drug potentiates the cytotoxicity of US.[21,22] The potentiation of some anticancer agents occurs when the agent may become more potent against the tumor cells when used in conjunction with US. The absorption of ultrasound energy by the agent and the production of free radicals seem to be the likely mechanisms of this increase.[23,24] In order to assess the accelerated (synergistic) drug effect of angiogenesis inhibitor using US energy, this study examined for the first time the therapeutic effect of an angiogenesis inhibitor combined with US irradiation for human cancer *in vivo*. In addition, the effect of antiangiogenesis in this combined treatment was assessed non-invasively using color Doppler US in real-time with a microbubble contrast agent.

Materials and Methods

Cell line and nude mice. A human uterine sarcoma cell line, FU-MMT-1, previously established by us from a patient with uterine carcinosarcoma, was used in this study because this tumor is one of the most malignant neoplasms of the human solid tumors and it also has a poor response to any of the chemotherapeutic agents currently used, as well as to radiotherapy. FU-MMT-1 shows highly progressive activity both *in vitro* and *in vivo*. This

[4]To whom correspondence should be addressed. E-mail: emoto@cis.fukuoka-u.ac.jp

doi: 10.1111/j.1349-7006.2007.00474.x

cell line is chiefly composed of rhabdomyosarcoma cells and the immunophenotype, tumorigenicity, and cytogenetic characteristics have been reported previously.[14] Female BALB/cA Jcl-nu athymic nude mice were obtained from Clea (Tokyo, Japan). Five to 6-week-old mice weighing 20 g were used in the experiments. All animals were kept in isolation rooms at a controlled temperature and they were caged in groups of five of fewer and had free access to standard animal chow and water according to the Instructions of the Institute of Experimental Animal Science, Fukuoka University Medical School.

***In vitro* tube formation assay.** Experiments on tube formation were conducted in triplicate in 24-multiwell dishes using an Angiogenesis kit (Kurabo, Osaka, Japan), according to the manufacturer's instructions. Briefly, human umbilical vein endothelial cells (HUVEC) cocultured with human fibroblasts were cultivated with TNP-470 (1 μg/mL), FR118487 (1 μg/mL), and thalidomide (1 μg/mL) in the medium containing 10 ng/mL of vascular endothelial growth factor (VEGF). An angiogenesis inhibitor, FR118487 was synthesized by chemical modification of the fermentation products of a fungus, *Scolecobasidium arenarium* (F-2015), at Fujisawa Pharmaceutical Co., Ltd (Tsukuba, Japan). The medium was changed every 3 days. After 10 days, the dishes were washed with phosphate-buffered saline (PBS) and fixed with 70% ethanol at 4°C. After the fixed cells were rinsed three times with PBS, the cells were then incubated with mouse antihuman CD31 (Kurabo, Osaka, Japan) in PBS containing 1% bovine serum albumin (BSA) for 60 min. After washing with 1% BSA–PBS three times, the cells were incubated with goat antimouse IgG AlkP conjugate (Kurabo, Osaka, Japan). Metal-enhanced 3,3′-diamino-benzidine-tetrahydrochloride (DAB) was the substrate, the reaction yielding a dark reddish-brown insoluble end-product. Finally, the cells were washed with PBS five times, and viewed using an Olympus microscope. The area and tube length were measured using the Kurabo angiogenesis image analyzer (Kurabo, Osaka, Japan) in five different fields per each well, and then were statistically analyzed.

Chemicals. TNP-470 was kindly donated by Takeda Chemical Industries (Osaka, Japan). Its structure and characteristics have been described previously.[11] TNP-470 was suspended in a vehicle of 0.5% ethanol plus 5% gum arabic in saline. FR118487 was kindly donated by Fujisawa Pharmaceutical Co., Ltd (Tsukuba, Japan). The inhibitory effect of this drug on angiogenesis in the rabbit cornea has previously been described.[25]

Injection of TNP-470 and ultrasound irradiation. The mice were injected subcutaneously with 2×10^5 FU-MMT-1 cells in 0.2 mL DMEM in the right auxiliary region of the flank. Mice bearing the resultant tumors measuring 5–10 mm in diameter on the 14th day were randomly separated into four groups as follows: i) US irradiation alone ($n = 8$); ii) TNP-470 injection alone ($n = 8$); iii) combination of TNP-470 and US irradiation ($n = 8$), and iv) non-treatment as the control ($n = 12$: injection of 0.5% ethanol plus 5% gum arabic in saline) and these therapies were continued for 8 weeks. TNP-470 was injected subcutaneously at a dose of 30 mg/kg three times per week for each mouse in groups of TNP-470 alone and the combined treatment. The mice were anesthetized with ether and US (continuous wave, at 1 MHZ frequency, and 2.0 w/cm^2 intensity), was irradiated through a probe onto subcutaneous tumors for 4 min three times per week using Sonitron 1000 (Rich-mar, Inola, OK) for each mouse in groups of US alone and the combined treatment. Tumor growth was monitored by measuring the weekly volume twice, calculated as $V = a \times b^2/2$ (a = length; b = width). An autopsy was done on all mice soon after finishing these therapies or when they died during the course of therapies and the tumors were then harvested, and the size and the weights of these tumors were measured. Mean, SD, median, and SE of the tumor size during the courses and those of the tumor weight after the therapies in each group were calculated.

Evaluation of tumor vascularity with contrasted color Doppler US. The intratumoral vascularity in xenografts was examined after finishing each treatment using color Doppler US (SSD-4000, Aloka Ltd, Tokyo, Japan) with a 7.5-MHz curved array transducer (UST-987-7.5, Aloka Ltd) using a microbubble ultrasound contrast agent, Optison® (Molecular Biosystems Inc., San Diego, CA, USA) at our animal center in Fukuoka University. The US examinations were standardized using a medium wall filter, pulsed repetition frequency of 1000 Hz, moderate-to-long persistence, and a slow and steady movement of the transducer to achieve the highest sensitivity without apparent background noise. The intratumoral blood flow was enhanced after an i.v. bolus injection of Optison® (0.6 mL/kg). Optison® is approved for use in echocardiography by the USA Food and Drug Administration (FDA) and consists of a suspension of perfluoropropane-filled albumin microspheres with a concentration of 6.3×10^8 bubbles/mL. After the examination, the previously stored images were retrieved and displayed on the monitor. The area in the longitudinal image on the US monitor of each tumor was automatically calculated using the manual-trace measurement of the length of tumor circumference, then, the number of colored vessels within the tumor was counted. The average sonographic vascular density (ASVD) was calculated as the number of colored-vessels within a longitudinal tumor section divided by the area. The ASVD in each treatment group was calculated (±SD) and statistically compared. Moreover, the areas of highest neovascularization were then identified on their stored images. The tumor vessel counts over an area of 19.625-mm^2 (a field of a circle with 5 mm in diameter) per field in each of these three areas within the tumor were then counted as the highest sonographic vascular density (HSVD). The averages of the HSVD in the three 19.625-mm^2 fields of each tumor were calculated in each treatment group (±SD) and statistically compared.

Evaluation of tumor vascularity with immunohistochemistry. The paraffin sections from each tumor were reacted with each primary antibody for 1 h at room temperature in our pathology laboratory. The attached antibodies were visualized using the labeled streptavidin-biotin (LSAB) method (Zymed, San Francisco, CA, USA). The monoclonal antibody used was anti-CD34 (an endothelial marker: 1:50; Dako) for endothelial cells in the tumor vessels. The negative controls consisted of an omission of the primary antibody. Microvessel density (MVD) was measured in all tumors treated in this therapy. Intratumoral microvessels were highlighted using anti-CD34 immunostaining in formalin-fixed, paraffin-embedded sections in each tumor. The MVD quantitation in the highest vascularization (so-called hot spots) was examined in each tumor in the same manner as in our previous study,[26] which was named as the highest immunohistochemical MVD (HIMVD). The average of the HIMVD in these three groups and that in the controls was then calculated. Moreover, to assess the average vascularization in entire tumor sections, 10 areas were randomly chosen in each tumor then the tumor vessels were counted, and then the obtained density was considered to be the average immunohistochemical MVD (AIMVD).

Statistical analysis. These *in vivo* data were expressed as the mean ± SD. The Mann–Whitney *U*-test (non-parametric) was used to compare tumor growth, or tumor weight between three treatment groups and the control. The unpaired *t*-test (parametric) was used to compare tumor vessel density between three treatment groups and the control. These statistical analyses were done using the software package StatView 5.0 (SAS Institute, Inc., Cary, NC, USA) for Macintosh. The results were judged to be statistically significant if the *P*-value of each respective test statistic was less than 0.0001.

Results

***In vitro* tube formation assay.** To investigate the antiangiogenic effect of angiogenesis inhibitors, a tube formation assay was

doi: 10.1111/j.1349-7006.2007.00474.x

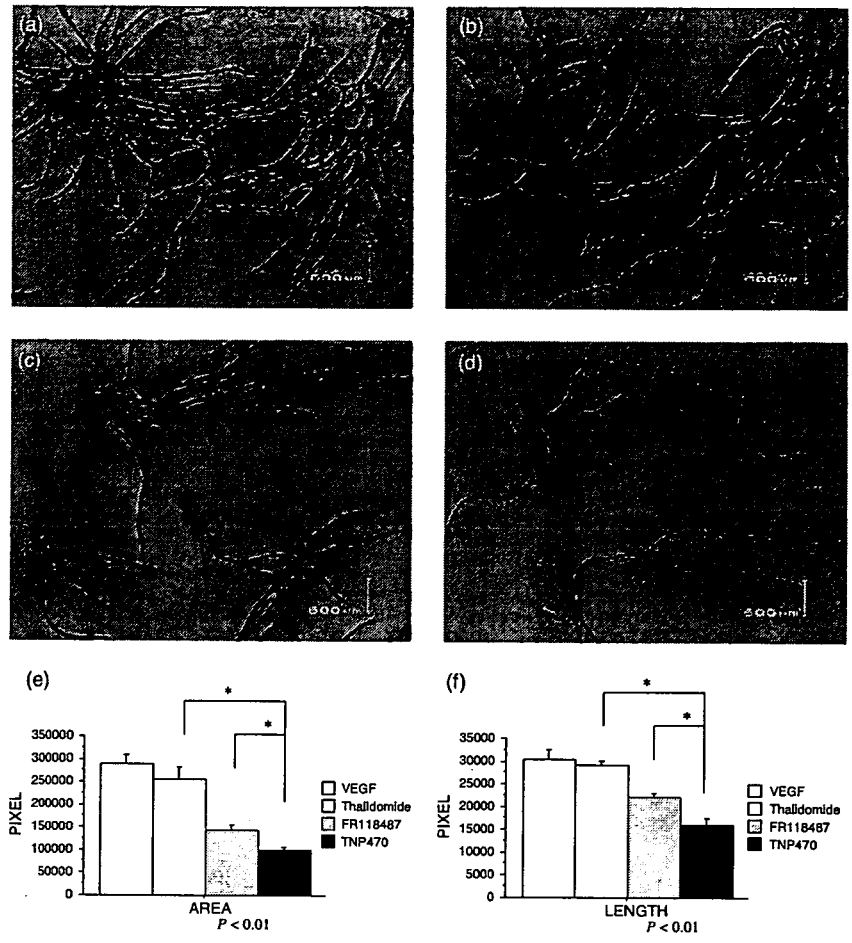

Fig. 1. (a–f) Effects on tube formation *in vitro*. (a) When human umbilical vein endothelial cells (HUVEC) were cultured in the presence of VEGF (10 ng/mL), efficient tube formation was observed. (d) TNP-470 (1 μg/mL) significantly inhibited the tube formation *in vitro*, in comparison to the other two antiangiogenic agents, (b) thalidomide (1 μg/mL) and (c) FR118487 (1 μg/mL), in quantitative analysis of both (e) tube area and (f) length using an image analyzer.

performed using HUVEC cocultured with human fibroblasts. When HUVEC were cultured in the presence of VEGF, efficient tube formation was observed (positive control). In a quantitative analysis of both tube area and length, TNP-470 significantly inhibited the tube formation *in vitro*, in comparison to the other two antiangiogenic agents, thalidomide, and FR118487 in this study ($P < 0.01$; Fig. 1a–f). We therefore finally selected TNP-470 to use in our following *in vivo* study as a representative agent.

Suppression of tumor growth. The weekly changes in the mean tumor volume in xenografts during the courses of therapies are shown in Fig. 2. Either treatment of US alone or TNP-470 alone inhibited the growth of the FU-MMT-1 xenografts, in comparison to that of the control (Mann–Whitney-*U*-test: $P = 0.151$, and $P = 0.006$). Furthermore, a significantly enhanced effect to suppress the tumor growth was obtained using the combined treatment (*vs* US alone: $P < 0.0001$; and *vs* TNP-470 alone: $P < 0.0001$; Fig. 1). No significant difference in the mean tumor volume was observed between the treatments using US alone and TNP-470 alone ($P = 0.176$).

The mean weight after treatment of either US alone (10.98 ± 2.27 g, range: 4.8–17.2 g) or TNP-470 alone (8.94 ± 3.07 g, range: 0.0–21.2 g) was smaller than that of the control (Mann–Whitney-*U*-test *vs* US alone: $P = 0.0042$; *vs* TNP-470 alone: $P = 0.025$). The enhanced effect of the weight reduction in xenografts was shown by the combined treatment (0.75 ± 0.52 g, range: 0.0–4.8 g), in comparison to either US alone ($P = 0.027$) or TNP-470 alone ($P = 0.050$). The mean weight of the xenografts measured after the combined treatment was significantly lower than that of the control (25.04 ± 3.85 g, range: 7.6–30.8 g; $P = 0.0007$; Fig. 3).

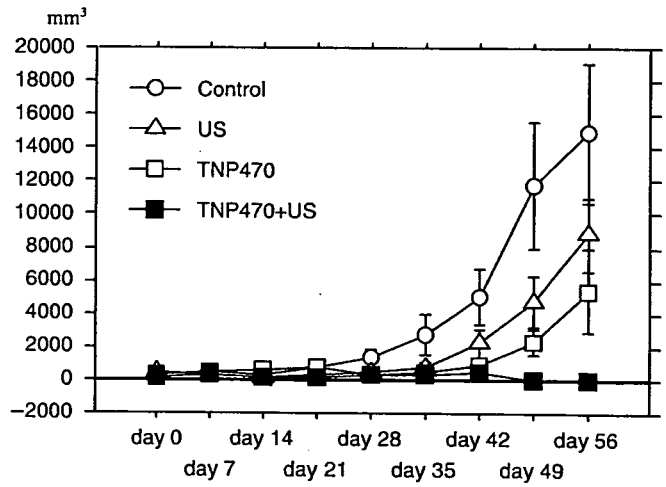

Fig. 2. Effects on growth of the FU-MMT-1 xenografts. Each curve represents the mean and SD of the tumor (mm³) volume in each group. Either treatment with ultrasound alone or TNP-470 alone significantly inhibited the growth of the FU-MMT-1 xenografts, in comparison to that of the non-treatment group (control; Mann–Whitney-*U*, $P = 0.151$, and $P = 0.006$). Moreover, a significantly enhanced effect was obtained using the combined treatment, in comparison to that of each therapy alone (Mann–Whitney-*U*, *vs* US alone: $P < 0.0001$, and *vs* TNP-470 alone: $P < 0.0001$).

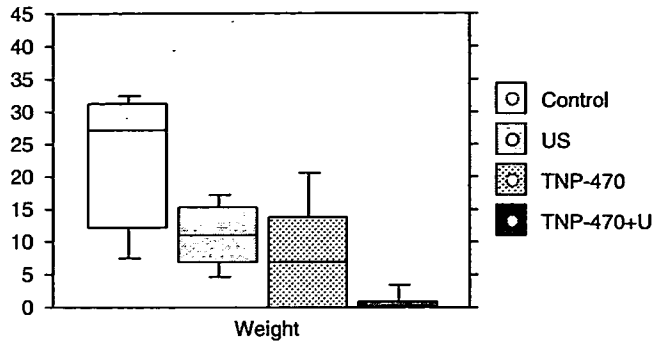

Fig. 3. The mean (SD) tumor weights (g) in the FU-MMT-1 xenografts resected after treatment. The mean tumor weight after treatment of either ultrasound (US) alone (10.98 ± 2.27 g, range: 4.8–17.2 g) or TNP-470 alone (8.94 ± 3.07 g, range: 3.1–21.2 g) was smaller than that of the control (25.04 ± 3.85 g, range: 7.6–30.8 g; Mann–Whitney-*U*-test, *vs* US alone: $P = 0.0042$; *vs* TNP-470 alone; $P = 0.025$). The enhanced effect of the weight reduction in xenografts was shown by the combined treatment (0.75 ± 0.52 g, range; 0.0–4.8 g), in comparison to either US alone ($P = 0.027$) or TNP-470 alone ($P = 0.050$). The mean tumor weight of the xenografts measured after the combined treatment was significantly lower than that of the control ($P = 0.0007$).

After these treatments, disappearance of the tumor (tumor free) was seen in five of eight (62.5%) mice in the combined treatment, and two of eight (25.0%) in TNP-470 alone (χ^2 test; $P = 0.13$), whereas no such disappearance was seen after US alone, or in the control (*vs* combined treatment: $P = 0.007$, and $P = 0.001$). Dissemination, or direct invasion into the abdominal cavity by the tumor was only seen in the control (33.3%; four of 12 mice).

Evaluation of the antiangiogenic effect using contrast color Doppler ultrasound. The effects of antiangiogenesis for FU-MMT-1 xenografts by these therapies were evaluated using contrast Doppler US in real-time after the 8 weeks of treatment (Fig. 4a–d). In the evaluation with ASVD, the mean of the group of combination treatment was significantly lower than that of the control (unpaired *t*-test: $P = 0.04$), whereas no significant difference was observed between either the treatment of US alone or TNP-470 alone and the control ($P = 0.39$, $P = 0.41$). In the evaluation with HSVD, the mean of the group of either TNP alone or combination treatment was thus significantly lower than that of the control (unpaired *t*-test: $P = 0.002$, $P = 0.000004$), whereas no significant difference was observed between the treatment of US alone and the control ($P = 0.16$). The reduction in the vascular density (HSVD) was significantly enhanced by the combined treatment, in comparison to that of the US treatment alone ($P = 0.0003$), or the TNP-470 alone ($P = 0.00009$; Table 1). The intratumoral vascularity could not be fully evaluated

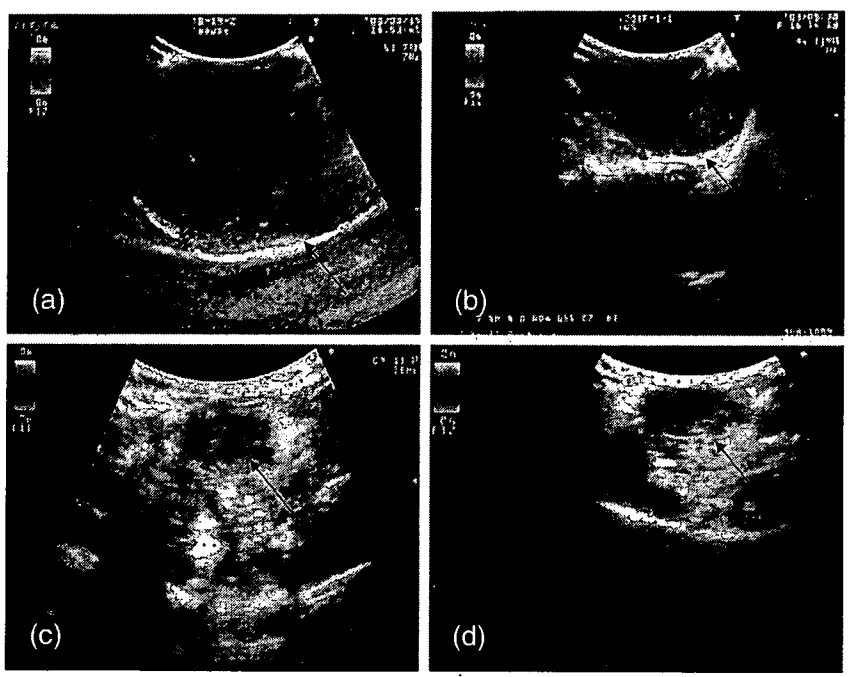

Fig. 4. (a–d) Visualization of the intratumoral blood flow using non-invasive contrasted color Doppler ultrasound (US) in FU-MMT-1 human uterine sarcoma growing subcutaneous on the backs of BALB/cA Jcl-nu mice. Representative Doppler ultrasound pictures are taken at maximal signal intensity after injecting the US contrast agent (10 s after injection). The tumor vessel density in (c) the group of TNP-470 treatment alone was lower than that of (a) the control (unpaired *t*-test, $P = 0.0007$), whereas no significant difference was observed between (b) the treatment of US alone and the control (unpaired *t*-test, $P = 0.11$). The reduction of tumor vessel density was significantly enhanced by (d) the combined treatment, in comparison to that of the US treatment alone ($P = 0.00002$), or the TNP-470 alone (unpaired *t*-test, $P = 0.00009$).

Table 1. The sonographic and immunohistochemical vascular density in FU-MMT-1 xenografts after 8 weeks' treatments

	Control	US alone	TNP-470 alone	TNP-470 + US
1) Average sonographic vascular density (per 100 mm²)	8.6 ± 2.1	7.7 ± 2.0	7.6 ± 2.3	**5.5 ± 1.3**
2) Highest sonographic vascular density (per 19.63 mm²)	14.6 ± 1.8	12.9 ± 2.7	**11.1 ± 1.4**	**3.6 ± 1.1**
3) Average immunohistochemical microvessel density†	49.8 ± 10.2	**25.9 ± 12.1**	**25.1 ± 14.1**	**9.4 ± 3.2**
4) Highest immunohistochemical microvessel density†	61.3 ± 10.7	60.8 ± 14.7	50.8 ± 13.7	**11.3 ± 2.2**

†Per high-power field (0.74 mm²). 1) Control versus US: $P = 0.39$, or TNP-470: $P = 0.41$, or TNP-470 + US: $P = 0.04$. TNP-470 versus TNP-470 + US: $P = 0.19$. 2) Control versus US: $P = 0.16$, or TNP-470: $P = 0.002$, or TNP-470 + US: $P = 0.000004$. TNP-470 + US versus US alone: $P = 0.0003$, or TNP-470: $P = 0.00009$. 3) Control versus US: $P = 0.0008$, or TNP-470: $P = 0.002$, or TNP-470 + US: $P = 0.0001$. TNP-470 + US versus US alone: $P = 0.05$, or $P = 0.04$. 4) Control versus US: $P = 0.94$, or TNP-470: $P = 0.13$, or TNP-470 + US: $P = 0.000002$. TNP-470 + US versus US alone: $P = 0.0001$, or TNP-470 alone: $P = 0.001$. Bald: $P<0.05$ (versus control).

doi: 10.1111/j.1349-7006.2007.00474.x

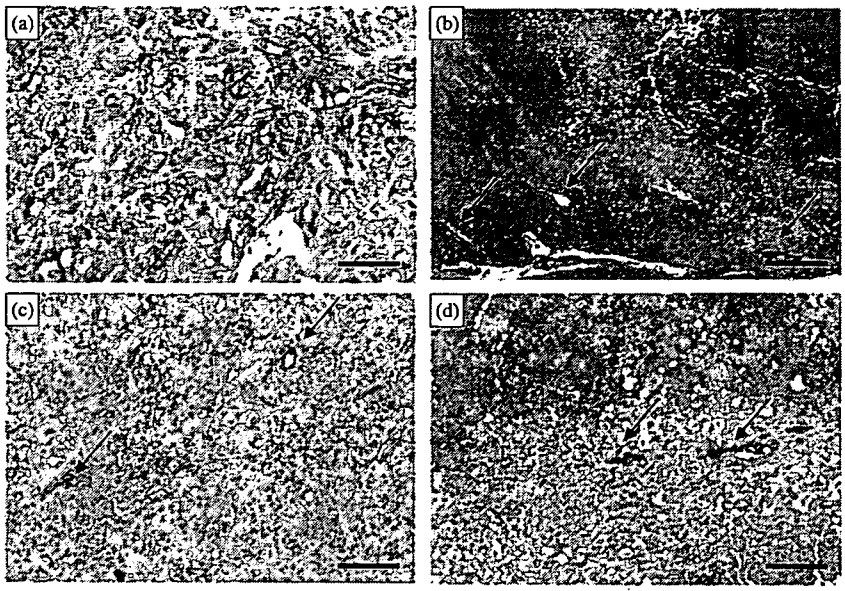

Fig. 5. (a–d) Intratumoral microvessels immunohistochemically stained (red colored) by anti-CD34. The tumor vessel densities in both groups of (b) ultrasound (US) alone and (c) TNP-470 treatment alone were significantly lower than that of (a) the control. The reduction of tumor vessel density was significantly enhanced by (d) the combined treatment, in comparison to that of (b) the US treatment alone, or (c) the TNP-470 alone. The destruction of tumor vessels (→) and areas of coagulative necrosis (upper areas in both b and d) are apparently shown in either US treatment alone or after combination treatment. Scale bars: 200 μm.

using either non-contrasted color Doppler or power Doppler ultrasound because the intensity of the signals of the colored-blood flow in these approaches were apparently lower than that of contrasted color Doppler ultrasound.

MVD. The mean of AIMVD in each treatment group was significantly lower than that of the control (unpaired *t*-test, US: $P = 0.0008$; TNP-470: $P = 0.002$; combination: $P = 0001$). The reduction of AIMVD was significantly enhanced by the combined treatment, in comparison to that of the TNP-470 treatment alone ($P = 0.04$). In contrast, no difference in the mean of HIMVD was observed between the group of either US treatment alone or TNP-470 treatment alone and the control ($P = 0.94$, $P = 0.13$). However, the reduction of HIMVD was significantly enhanced by the combined treatment, in comparison to that of the US treatment alone ($P = 0.0001$), or the TNP-470 alone ($P = 0.001$; Table 1; Fig. 5a–d). The destruction of the tumor vessels and areas of coagulative necrosis were apparently seen in tumors of either US therapy alone or combination treatment, in comparison to either the control or TNP-470 treatment alone group.

Toxicity. No side-effect such as a loss of body weight, or neurotoxicity was significantly observed in any mice in this study.

Discussion

TNP-470 blocks endothelial cell cycle progression in the late G1 phase to activate p53 in endothelial cells, thus leading to an increase in cyclin-dependent kinase inhibitor $p21^{CIP/WAF}$ expression and subsequent growth arrest.[10] The molecular target of TNP-470 has been found to be MetAP-2, an intracellular enzyme necessary for the process of protein myristolation, thus preventing membrane proteins from translocating to the cell surface.[9] Moreover, TNP-470 suppresses the production of bFGF, or VEGF *in vitro*.[5,13] TNP-470 has been shown to act for human malignancies as a single agent in a wide variety of preclinical models[11–13] and some clinical trials.[27,28] Recent studies have showed a synergistic effect of radiation and angiogenesis inhibitors.[6,7] The combination of angiostatin, an antiangiogenic agent, and radiotherapy has been shown to work best when angiostatin was given simultaneously with radiotherapy *in vivo*.[6] The successful outcome from the combination of TNP-470 with cytotoxic therapies[5] or radiotherapy[15] has been also shown *in vivo*.

Weight loss has been frequently observed in animals receiving TNP-470, and the dose-limiting neurotoxicity associated with TNP-470 has been reported in clinical trials.[28] In the present study, the dose of TNP-470 was thus kept low (30 mg/kg/day, three times/week), so that no remarkable side-effects were observed in any mice treated using TNP-470 with or without US irradiation. To reduce the toxicity of TNP-470, however, a recent study tried using water-soluble synthetic polymers, *N*-(2-hydroxypropyl) methacrylamide (HPMA) copolymer, as a specific carrier of TNP-470, so that this HPMA copolymer-TNP-470 substantially enhanced and prolonged the activity of TNP-470 *in vivo* and did not cause any weight loss or neurotoxic effects in mice.[29] Further approaches or new ideas may be required to reduce the toxicity of antiangiogenic agents.

US, which is routinely used for diagnostic imaging applications, is now being adopted in various therapeutic applications. The effect of US in activating antitumor drugs or agents has been studied both *in vitro* and *in vivo*.[16,17,19] Our previous study showed that leukemia cells could be selectively eliminated using low-intensity US in the presence of photosensitive drugs.[22] The mechanism behind the augmentation of the activity of anticancer drugs and other agents by US remains to be fully elucidated; however, several mechanisms have been suggested: i) increased permeability: the increased intracellular concentration of drugs after ultrasonic irradiation suggests an increased permeability (also called sonoporation), or the opening of pores in the cells.[20] Sonoporation is the term used for the phenomenon by which US may transiently alter the structure of the cellular membrane, thus inducing an enhanced uptake of low- and high-molecular-weight molecules into the cell. There have been a large number of studies in which a synergistic effect between US and different drugs has been sought. Regarding the mechanisms of action in an *in vitro* environment, acoustic cavitation and streaming may be predominant.[30] Our previous study showed that a direct observation of the cells using electron microscopy confirmed the presence of pore-like disruptions in the cell membrane after the combined treatment;[21] ii) increased sensitivity of the cells to the agent: US alone can cause lethal or sublethal cellular damage.[31] Interestingly, our current study also showed that US alone could inhibit the growth of a FU-MMT-1 xenograft established from a uterine sarcoma,[14] which is one of the most aggressive tumors among the human malignancies. Moreover, histopathologically, the destruction of tumor vessels and area of coagulative necrosis were apparently seen in tumors treated with either US therapy alone or combination treatment, compared to those treated with

TNP-470 therapy alone, thus suggesting direct cellular damage by US irradiation. One commonly observed vascular effect, usually characterized by an increased tumor blood flow during the initial period of therapeutic US irradiation and eventual destruction of the vasculature, renders the tumor mass more hypoxic.[31] Our current study supported the vascular effect of US *in vivo* because the mean AIMD in US treatment alone was significantly lower than that of control, and destruction of tumor vessels was apparently seen in the US treatment group. A recent study showed that malignant cells were found to be sensitive to therapeutic US treatment, thus resulting in a transient decrease in cell proliferation.[32] In a suspension of carcinoma cells exposed to 1 MHz ultrasound, cell killing was induced, accompanied by DNA strand breaks. This might be mainly attributable to free radical formation and the pyrolyitic processes.[24] Cells damaged sublethally by US are thus suggested to be more biologically susceptible to the antitumor agents; iii) potentiation of the agent: it is also suggested that anticancer agents became more potent against tumor cells when they are used in conjunction with US.[16,17,19] The absorption of US energy by the agent and the production of free radicals have been cited as the likely mechanisms of this increase.[33] Inertial cavitation is required in this process, primarily in the production of free radicals.[18] We thus irradiated with low-intensity US within a few minutes after the subcutaneous injection of TNP-470 to accelerate the drug potentiation because the mean plasma half-life of TNP-470 has been reported to be short (2–6 min in humans by intravenous injection).[28] As a result, this combined treatment could significantly inhibit the growth of FU-MMT-1 *in vivo*, in comparison to either TNP-470 used alone or US alone, thus suggesting an accelerated (booster, or synergistic) effect of US for TNP-470. We suppose that the possible mechanism of our combination therapy using a low-intensity US might be chiefly the first mechanism (sonoporation) described above.

As TNP-470 has been shown to possess antiproliferation effects for not only endothelial cells but also for tumor cells, the uptake of this agent might thus be enhanced in both cells by sonoporation. In addition, direct cellular damage including a vascular effect by US irradiation (the second mechanism) might be added because of the evidence of wide areas of coagulative necrosis in irradiated tissue specimens. Feril *et al.* recently reported monocytic leukemia cells (U937) were killed by combining hyperthermia sensitive drug, 2,2′-azobis (2-amidinopropane) dihydrochloride (AAPH) and exposure to non-thermal 1 MHz US for 1 min at an intensity of 2.0 W/cm^2.[34] Apoptosis measured using flow cytometry and free radical investigation using electron paramagnetic resonance (EPR) spin trapping showed that US-induced cell lysis and apoptosis were enhanced in the presence of AAPH, regardless of the temperature at the time of sonication. Although free radicals were increased in the combined treatment, this increase did not correlate well with cell killing.[34] The mechanism of enhancement pointed to the increased uptake of the agent during sonication rather than potentiation by AAPH. However, direct measurement of free radicals in the present experiment was technically impossible and further analysis will be needed to affirm these suppositions.

US has been used as a modality for diagnostic imaging in various clinical fields without producing any significant adverse effects. The neovascularization of tumors could be displayed using color Doppler US in various human solid tumors. The changes in intratumoral vascularity in xenotransplanted tumors treated using antiangiogenesis have been demonstrated using color Doppler US in real-time.[35,36] In our recent clinical report, using color Doppler US with a microbubble contrast agent was shown to enhance the vascularity of solid tumors, even in small lesions.[37] In the present study, the outcome of antiangiogenic treatment thus could be more efficiently evaluated using contrast color Doppler US than non-contrast Doppler. Our histopathological results supported the findings of sonographic vascular density and, immunohistochemically, both HIMVD and AIMVD in the combined treatment group were significantly lower than those in the TNP-470 treatment alone group. The discrepancy in the results between the HIMVD and AIMVD in US treatment alone as well as in TNP-470 treatment alone might be the result of the alternative angiogenesis (increased vascularity) focally seen near the hypoxic areas. In the present study, although a difference in the results of vascular density between color Doppler sonography and immunohistochemical examination was partially observed, another recent study has also showed the usefulness of contrast color Doppler to assess angiogenesis without an immunohistochemical examination *in vivo*.[35] Moreover, another study additionally reported that the color Doppler vascularity index is a better indicator of tumor behavior than the immunohistochemical microvessel density in colon cancer patients.[38] As a result, the combined treatment of TNP-470 and US irradiation was found to be more effective in suppressing angiogenesis for uterine sarcoma xenografts than either therapy alone. The mechanisms of this antiangiogenic therapy using low-intensity US for intratumoral microvessels as well as feeding vessels into the tumors therefore need to be more precisely elucidated.

The xenotransplanted model used in this study is originated from a human uterine carcinosarcoma,[14] which is one of the highest angiogenic tumors in all human solid malignancies. Our previous studies apparently showed higher expressions of VEGF-A and angiopoietin-2 genes as well as a higher frequency of lymphovascular invasion and a high-MVD of these tumors, in comparison to those of the other human uterine carcinomas.[26,39] As a result, the success of the antiangiogenic combination therapy used in the present study might therefore be associated with the high angiogenic activities (vascular-rich) of this tumor. Further trials of this combination therapy for other tumor models with either moderate or low levels of angiogenic activity might therefore be needed.

In conclusion, our results support the positive interaction between TNP-470 and US energy regarding the inhibition of growth, and angiogenesis of human uterine sarcoma. As a result, US irradiation is thus suggested to have enhanced the effect in antiangiogenesis therapy on this tumor, and this combination might be potentially useful for a new cancer therapy.

Acknowledgments

This research was partly supported by a grant from the Ministry of Education, Science and Culture, Japan (#11671164). A part of the content in this study was orally announced by the first author as the 'Effect of antiangiogenesis drug therapy combined with ultrasound irradiation for uterine cancer evaluated with contrasted ultrasonography' at the 14th World Congress on Ultrasound in Obstetrics and Gynecology at Stockholm, Sweden, September 4, 2004.

References

1 Folkman J. Tumor angiogenesis: Therapeutic implications. *N Engl J Med* 1971; **285**: 1182–6.
2 Carmeliet P, Jain RK. Angiogenesis in cancer and other diseases. *Nature* 2000; **407**: 249–57.
3 Willett CG, Boucher Y, di Tomaso E *et al.* Direct evidence that the VEGF-specific antibody bevacizumab has antivascular effects in human rectal cancer. *Nat Med* 2004; **10**: 145–7.
4 Herbst RS, Madden TL, Tran HT *et al.* Safety and pharmacokinetic effects of TNP-470, an angiogenesis inhibitor, combined with paclitaxel in patients with solid tumors: evidence for activity in non-small-cell lung cancer. *J Clin Oncol* 2002; **20**: 4440–7.
5 Inoue K, Chikazawa M, Fukata S, Yoshikawa C, Shuin T. Docetaxel enhances the therapeutic effect of the angiogenesis inhibitor TNP-470 (AGM-1470) in metastatic human transitional cell carcinoma. *Clin Cancer Res*, 2003; **9**: 886–99.
6 Gorski DH, Mauceri HJ, Salloum RM *et al.* Potentiation of the antitumor

doi: 10.1111/j.1349-7006.2007.00474.x

effect of ionizing radiation by brief concomitant exposures to angiostatin. *Cancer Res* 1998; **58**: 5686–9.
7 Mauceri HJ, Hanna NN, Beckett MA *et al.* Combined effects of angiostatin and ionizing radiation in antitumour therapy. *Nature* 1998; **394**: 287–91.
8 Ingber D, Fujita T, Kishimoto S *et al.* Synthetic analogues of fumagillin that inhibit angiogenesis and suppress tumour growth. *Nature (Lond)*, 1990; **348**: 555–7.
9 Zhang Y, Griffith EC, Sage J, Jacks T, Liu JO. Cell cycle inhibition by the anti-angiogenic agent TNP-470 is mediated by p53 and p21WAF1/CIP1. *Proc Natl Acad Sci USA* 2000; **97**: 6427–32.
10 Sin N, Meng L, Wang MQ, Wen JJ, Bornmann WG, Crews CM. The anti-angiogenic agent fumagillin covalently binds and inhibits the methionine aminopeptidase, MetAP-2. *Proc Natl Acad Sci USA* 1997; **94**: 6099–103.
11 Yanase T, Tamura M, Fujita K, Kodama S, Tanaka K. Inhibitory effect of angiogenesis inhibitor TNP-470 on tumor growth and metastasis of human cell lines in vitro and in vivo. *Cancer Res* 1993; **53**: 2566–70.
12 Yoshida T, Kaneko Y, Tsukamoto A, Han K, Ichinose M, Kimura S. Suppression of hepatoma growth and angiogenesis by a fumagillin derivative TNP 470. *Cancer Res* 1998; **58**: 3751–6.
13 Miura S, Emoto M, Matsuo Y, Kawarabayashi T, Saku K. Carcinosarcoma-induced endothelial cells tube formation through KDR/Flk-1 is blocked by TNP-470. *Cancer Lett* 2004; **203**: 45–50.
14 Emoto M, Iwasaki H, Kikuchi M *et al.* Two cell lines established from mixed Müllerian tumors of the uterus: Morphological, immunocytochemical, and cytogenetic analyses. *Cancer* 1992; **69**: 1759–68.
15 Lund EL, Bastholm L, Kristjansen PE. Therapeutic synergy of TNP-470 and ionizing radiation: effects on tumor growth, vessel morphology, and angiogenesis in human glioblastoma multiforme xenografts. *Clin Cancer Res* 2000; **6**: 971–8.
16 Saad AH, Hahn GM. Ultrasound enhanced drug toxicity on Chinese hamster ovary cells *in vitro*. *Cancer Res* 1989; **49**: 5931–4.
17 Loverock P, ter Haar G, Ormerod MG, Imrie PR. The effect of ultrasound on the cytotoxicity of adriamycin. *Br J Radiol* 1990; **63**: 542–6.
18 Worthington AE, Thompson J, Rauth AM, Hunt JW. Mechanism of ultrasound enhanced porphyrin cytotoxicity. Part I. A search for free radical effects. *Ultrasound Med Biol* 1993; **19**: 123–5.
19 Tomizawa M, Ebara M, Saisho H, Sakiyama S, Tagawa M. Irradiation with ultrasound of low output intensity increased chemosensitivity of subcutaneous solid tumors to an anti-cancer agent. *Cancer Lett* 2001; **173**: 31–5.
20 Brayman AA, Coppage ML, Vaidya S, Miller MW. Transient poration and cell surface receptor removal from human lymphocytes in vitro by 1 MHz ultrasound. *Ultrasound Med Biol* 1999; **25**: 999–1008.
21 Tachibana K, Uchida T, Ogawa K, Yamashita N, Tamura, K. Induction of cell-membrane porosity by ultrasound. *Lancet* 1999; **353**: 1409.
22 Tachibana K, Uchida T, Hisano S, Morioka E. Eliminating adult T-cell leukaemia cells with ultrasound. *Lancet* 1997; **349**: 325.
23 Tata D, Hahn G, Dunn F. Ultrasonic absorption frequency dependence of two widely used anti-cancer drugs: doxorubicin and daunorubicin. *Ultrasonics* 1993; **31**: 447–50.
24 Misik V, Riesz P. Free radical intermediates in sonodynamic therapy. *Ann NY Acad Sci* 2000; **899**: 335–48.
25 Otsuka T, Ohakawa T, Shibata T *et al.* A new potent angiogenesis inhibitor, FR118487. *J Microbiol Biotechnol* 1991; **1**: 163–8.
26 Emoto M, Iwasaki H, Ishiguro M *et al.* Angiogenesis in carcinosarcomas of the uterus: differences in the microvessel density and expression of vascular endothelial growth factor between the epithelial and mesenchymal elements. *Hum Pathol* 1999; **30**: 1232–41.
27 Kudelka AP, Verschraegen CF, Loyer E. Complete remission of metastatic cervical cancer with the angiogenesis inhibitor TNP-470. *N Eng J Med* 1998; **338**: 991–2.
28 Bhargava P, Marshall JL, Rizvi N *et al.* A phase I and pharmacokinetic study of TNP-470 administered weekly to patients with advanced cancer. *Clin Cancer Res* 1999; **5**: 1989–95.
29 Satchi-Fainaro R, Puder M, Davies JW *et al.* Targeting angiogenesis with a conjugate of HPMA copolymer and TNP-470. *Nat Med* 2004; **10**: 255–61.
30 Ter Haar G. Therapeutic applications of ultrasound. *Prog Biophys Mol Biol* 2007; **93**: 111–29.
31 Longo FW, Longo WE, Tomashefsky P, Lattimer JK, Rivin BD, Tannenbaum M. Interaction of ultrasound with neoplastic tissue. Local effect on subcutaneously implanted Furth-Columbia rat Wilms' tumor. *Urology* 1975; **6**: 631–4.
32 Yang R, Reilly CR, Rescorla FJ *et al.* High-intensity focused ultrasound in the treatment of experimental liver cancer. *Arch Surg* 1991; **126**: 1002–9.
33 Nicolai H, Steinbach P, Knuechel-Clarke R *et al.* Proliferation of tumor spheroids after shock-wave treatment. *J Cancer Res Clin Oncol* 1994; **120**: 438–41.
34 Feril LB Jr, Kondo T, Zhao QL *et al.* Enhancement of ultrasound-induced apoptosis and cell lysis by echo-contrast agents. *Ultrasound Med Biol* 2003; **29**: 331–7.
35 Gee MS, Saunders HM, Lee JC *et al.* Doppler ultrasound imaging detects changes in tumor perfusion during antivascular therapy associated with vascular anatomic alterations. *Cancer Res* 2001; **61**: 2974–82.
36 Abdollahi A, Lipson KE, Sckell A *et al.* Combined therapy with direct and indirect angiogenesis inhibition results in enhanced antiangiogenic and antitumor effects. *Cancer Res* 2003; **63**: 8890–8.
37 Emoto M, Fujimitsu R, Iwasaki H, Kawarabayashi T. Diagnostic challenges in patients with tumors: case 3. A normal-sized ovarian cancer detected by color Doppler ultrasound using a microbubble contrast agent. *J Clin Oncol* 2003; **21**: 3703–5.
38 Chen C-N, Cheng Y-M, Liang J-T *et al.* Color Doppler vascularity index can predict distant metastasis and survival in colon cancer patients. *Cancer Res* 2000; **60**: 2892–7.
39 Emoto M, Charnock-Jones DS, Licence D *et al.* Localisation of the VEGF and angiopoietin genes in uterine carcinosarcoma. *Gynecol Oncol* 2004; **95**: 474–82.

Increased Chemotherapeutic Activity of Camptothecin in Cancer Cells by siRNA-Induced Silencing of WRN Helicase

Kazunobu FUTAMI, Motoki TAKAGI,[1] Akira SHIMAMOTO,[2] Masanobu SUGIMOTO, and Yasuhiro FURUICHI*

GeneCare Research Institute Co., Ltd.; 19–2 Kajiwara, Kamakura, Kanagawa 247–0063, Japan.
Received May 10, 2007; accepted July 19, 2007

Werner syndrome helicase (WRN) participates in a wide range of DNA activities, including replication, double-strand DNA break repair, telomere and retrovirus long terminal repeat maintenance. Mutations of the *WRN* gene cause Werner syndrome (WS), an autosomal recessive premature ageing disorder associated with various symptoms related to ageing. In this study, we investigated the siRNA that specifically down-regulates WRN expression. WRN silencing increased markedly the chemotherapeutic activity of camptothecin (CPT) on cancer cells in terms of the extent of efficacy and lowering effective drug dosage, accompanied by suppressing recovery from DNA damage caused by CPT. Here, we propose a potential combination therapy of *WRN*-siRNA and CPT, looking forward to minimizing the inevitable adverse effects associated with cancer chemotherapy.

Key words Werner helicase; camptothecin; siRNA; anti-cancer drug

Werner syndrome (WS) is an autosomal recessive disorder causing symptoms of premature ageing.[3] In 1996, the Werner syndrome gene (*WRN*) responsible for WS was identified.[4] The gene product, WRN, acts as a DNA helicase (WRN helicase) with exonuclease activity.[5] WRN greatly participates in DNA metabolism by facilitating cellular processes, including DNA replication, recombination, repair, and transcription in cooperation with other cellular proteins. WRN may participate in the retrovirus replication.[6] WS patients lack functional WRN mainly because of mutations that cause premature termination in WRN synthesis, produce incomplete WRN molecules lacking C-terminal nuclear localization signals and so result in impaired nuclear transportation of WRN.[7]

The genotoxic clastogen 4-nitroquinoline-1-oxide (4NQO) induces a more distinct increase in both break and interchange aberrations in WS patient cells than in control cells from normal individuals or from patients with other diseases.[8] WS patient lymphoblastoid cell lines (LCLs) transformed by Epstein-Barr virus are hypersensitive to 4NQO than LCLs from normal individuals without mutation.[9] Previously we studied the effect of camptothecin (CPT), a DNA topoisomerase I-trapping agent, on several LCLs from non-WS individuals and WS patients, and showed that CPT had a stronger cytotoxic effect on LCLs from WS patients than LCLs from non-WS individuals.[10] Poot *et al.* confirmed and extended our results by showing that CPT more strongly impairs S-phase transit in WS LCLs than in normal LCLs.[11] Lebel and Leder made homozygous WS embryonic stem cells (ES) of mice that lacked normal *WRN* genes at both alleles.[12] Such cells were more markedly sensitive to CPT than were wild-type ES cells.

From these results, we investigated if silencing *WRN* gene expression by siRNA targeting the *WRN* gene (*WRN*-siRNA) increases the sensitivity of cells against CPT. We show here that specific down-regulation of WRN expression increases the cytotoxic effects of CPT in cancer cells, and we discuss the potential of using these findings for cancer therapy.

MATERIALS AND METHODS

Cell Culture and Transfection HeLa cells were cultured in Dulbecco's modified Eagle's medium (Sigma, St. Louis, MO, U.S.A.) supplemented with 10% fetal calf serum and 25 μg/ml gentamicin (Sigma, St. Louis, MO, U.S.A.). Cells in 100 mm dishes were cultured at 37 °C in a humidified atmosphere containing 5% CO_2.

siRNA We preliminarily examined *WRN*-gene-silencing activity with several siRNA sequences by using down-regulations of *WRN* mRNA expression as a marker. The design of siRNAs was done according to the method of Elbashir *et al.*[13] The siRNAs used for silencing the target gene expression consisted of 21 bp duplexes complementary to a unique sequence of the target gene. All these siRNAs had an extra dTdT overhang at their 5′ ends. Among them, *WRN*-siRNA with the following sequence was the most effective in silencing WRN expression that suppressed the expression of *WRN* mRNA by more than 80% in HeLa cells: GUUCUUGUCACGUCCUCUG targeted against 3373—3391 bases of NM000553. Our intensive homology search by using Smith and Waterman method showed that no other human sequence was identical to this sequence except for the *WRN* gene. We used this *WRN*-siRNA in this study. As a negative control, a non-silencing siRNA duplex (*NS*-siRNA) having sequence 5′-UUCUCCGACGUGUCACGUdTdT-3′ was used. Both of these siRNAs were synthesized by using Qiagen-Xeragon (Germantown, MD, U.S.A.). Transfection of cells with these siRNAs (10 nM) was done by using Oligofectamine (Invitrogen, CA, U.S.A.).

Immunoblotting Cells were washed with ice-cold PBS, were pelleted and then were lysed in a sodium dodecyl sulfate (SDS) buffer containing 1% SDS, 2% beta-mercaptoethanol, 20% glycerol, 30 mM Tris–HCl (pH 6.8), and 0.2 M dithiothreitol. The cell lysate was boiled for 5 min and was electrophoresed on 7.5% SDS-polyacrylamide gels. Proteins fractionated on the gels were electrophoretically transferred to polyvinylidene difluoride membranes (Immobilon, Millipore, MA, U.S.A.) and were blocked overnight with 5% skimmed milk in PBS. Then the membranes were incubated

* To whom correspondence should be addressed. e-mail: furuichi@genecare.co.jp

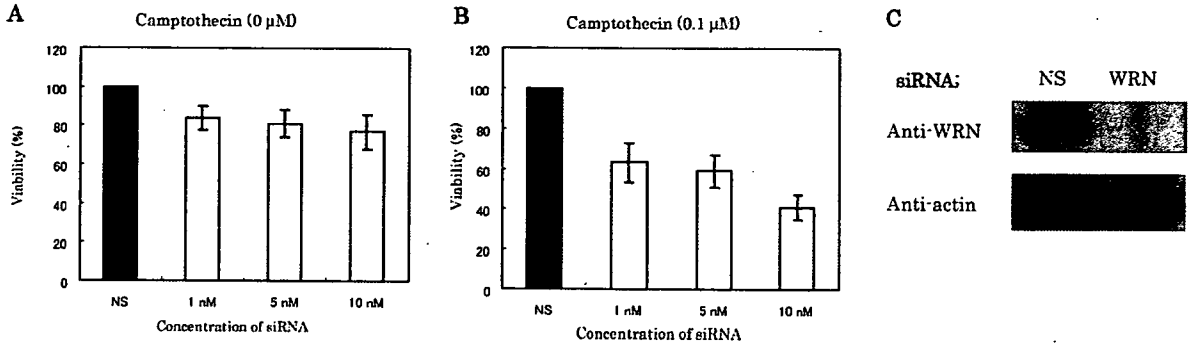

Fig. 1. Dose Effect of *WRN*-siRNAs to Increase CPT-Induced Cytotoxicity in HeLa Cells

The percentage of viability is expressed by viability with *WRN*-siRNA/viability with *NS*-siRNA×100. (A) Percentage of viability determined at 72 h after transfection with *WRN*-siRNAs and *NS*-siRNAs at concentrations 1, 5 and 10 nM, without CPT. (B) Percentage of viability determined at 72 h after transfection with *WRN*-siRNA and *NS*-siRNA at concentrations 1, 5 and 10 nM, in the presence of 0.1 μM CPT added 24 h after transfection. (C) Effect of *WRN*-siRNA (10 nM) on WRN expression levels in HeLa cells assessed by immunoblot analysis. Cell lysates (10 μg) were applied to each lane. Vertical bars indicate standard errors.

with either anti-WRN (4H12)[14] or anti-β-actin monoclonal antibodies (ICN Biomedicals, Aurora, Ohio, U.S.A.) for 60 min at room temperature, were washed with 0.05% Tween-20 in PBS, were incubated with anti-mouse IgG conjugated with horse radish peroxidase (DakoCytomation, Carpinteria, CA, U.S.A.) and then were washed and developed using an enhanced chemiluminescence reagent (ECL) plus (Amersham Biosciences, U.K.).

Confocal Microscopy HeLa cells cultured at 37 °C on microscope cover slips were transfected with 10 nM of *NS*- or *WRN*-siRNA, and were cultured further for 30 h. Then the culture medium was replaced with fresh medium containing 10 μM CPT (Sigma, OR, U.S.A.) and the cells were cultured for 6 h. Then, some CPT-treated cells were cultured in the absence of CPT for an additional 3 h to recover from the CPT effect, were fixed with a 3.7% formaldehyde PBS solution at room temperature for 10 min, and then were permeabilized with a 0.1% Triton X-100 PBS solution for 5 min. To detect WRN helicase and replication protein A (RPA), the cells were blocked by incubating in a 3% skimmed milk PBS solution for 60 min and were incubated overnight with primary antibodies (anti-RPA34; Oncogene, Boston, MA, U.S.A.) at 4 °C. The slides were washed with 0.05% Tween-20 in PBS three times and were incubated with Alexa Fluor 488-conjugated antibody mouse IgG (Molecular Probes, Eugene, OR, U.S.A.) as a secondary antibody for 60 min at room temperature. Fluorescent images were visualized by using a confocal laser-scanning microscope (Fluoview II; Olympus, Tokyo, Japan).

Cytotoxicity Test To determine the sensitivity to CPT, HeLa cells cultured in 48-well plates were transfected with various doses of siRNA using Oligofectamine. After 24 h, the cells were incubated in Dulbecco's modified Eagle's medium containing various concentrations of CPT. After 48 h (*i.e.*, after 72 h starting from siRNA transfection), the cell viability was measured by using a WST-8 assay (Nacalai Tesque, Kyoto), a modified MTT assay.[15]

RESULTS AND DISCUSSION

siRNA-Mediated Suppression of WRN Expression Immunoblot analysis showed that treatment of HeLa cells with *WRN*-siRNA for 30 h almost completely suppressed WRN expression, but *NS*-siRNA added as a negative control

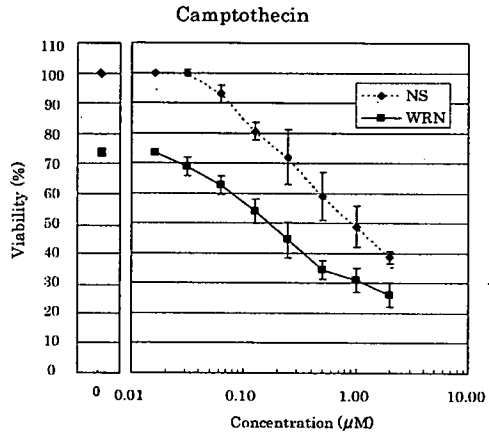

Fig. 2. Dose Effect of CPT to Induce Cytotoxicity in HeLa Cells in the Presence of *WRN*-siRNA

HeLa cells were transfected with *WRN*- or *NS*-siRNA at concentration 10 nM, and were treated with a serial dilutions of CPT added 24 h after transfection. After 48 h of culture, cell viability was monitored by WST-8 assay. The percentage of cell viability was expressed by cell viability in the presence of 10 nM *NS*-siRNA with various concentrations of CPT/cell viability in the presence of 10 nM *NS*-siRNA without CPT×100 (NS), and by cell viability in the presence of 10 nM *WRN*-siRNA with various concentrations of CPT/cell viability in the presence of 10 nM *NS*-siRNA without CPT×100 (WRN). Each point represents a mean of 9 samples and vertical bars indicate standard deviation.

did not affect the initial level of WRN (Fig. 1C). When the effect of 1, 5, 10 nM *WRN*-siRNAs on the growth of HeLa cells was examined by culturing the transfected cells for 96 h, *WRN*-siRNA alone weakly suppressed cell viability at these very low concentrations: cell viability was down-regulated by about 20% compared with cells treated with *NS*-siRNA (Fig. 1A). This reduction of the viable cell population might be mostly due to a delay in cell cycling as measured by flow cytometry analysis (unpublished observation). However, when *WRN*-siRNA-treated HeLa cells were incubated with CPT, cell viability was markedly reduced dependent on the dose of *WRN*-siRNA, and cells treated with *NS*-siRNA were totally unaffected (Fig. 1B).

We compared the cytotoxic dose of CPT with HeLa cells treated with 10 nM *NS*-siRNA and *WRN*-siRNA by changing the concentrations of CPT (Fig. 2). The IC_{50} of CPT was markedly decreased by 5.3-fold from 0.95 to 0.18 μM for *WRN*-siRNA-treated HeLa cells compared with the IC_{50} of CPT with *NS*-siRNA-treated HeLa cells. These results indicate that *WRN*-silenced HeLa cells were more susceptible to

CPT.

Failure of WRN-Silenced Cells to Recover from DNA Damage Response WRN in the nuclei is mainly in the nucleolus,[14,16] but it relocates to the nucleoplasm and colocalizes with RPA34 protein to form nuclear foci at the DNA double-strand break points that are generated by genotoxic reagents such as CPT.[17] The RPA34 protein does not bind to duplex DNA, but it binds to the single-strand regions of DNA unwound by DNA helicase for repair. Thus, nuclear foci consisting of WRN or RPA34 or both are assumed to be excellent markers representing damaged DNA loci generated by CPT treatment. Therefore, experiments were done to investigate how down-regulation of WRN affects nuclear RPA34 foci formation and DNA repair during the recovery process of DNA damage (double-strand breaks) caused by CPT. In the absence of CPT, most of WRN was found in the nucleolus while RPA34 was dispersed in the nucleoplasm as reported before[17] (Fig. 3A). Down-regulation of WRN expression by siRNA treatment, however, made some fraction of RPA34 form nuclear foci in the nucleoplasm (Fig. 3B). This nuclear relocation of RPA may be interpreted that RPA34 assemble in the legions of endogenous DNA damages which are formed during DNA replication and remain unrepaired due to the absence of WRN in the slightly delayed cell cycle progression as shown in Fig. 1A.

When HeLa cells were treated with CPT for 6 h, many nu-

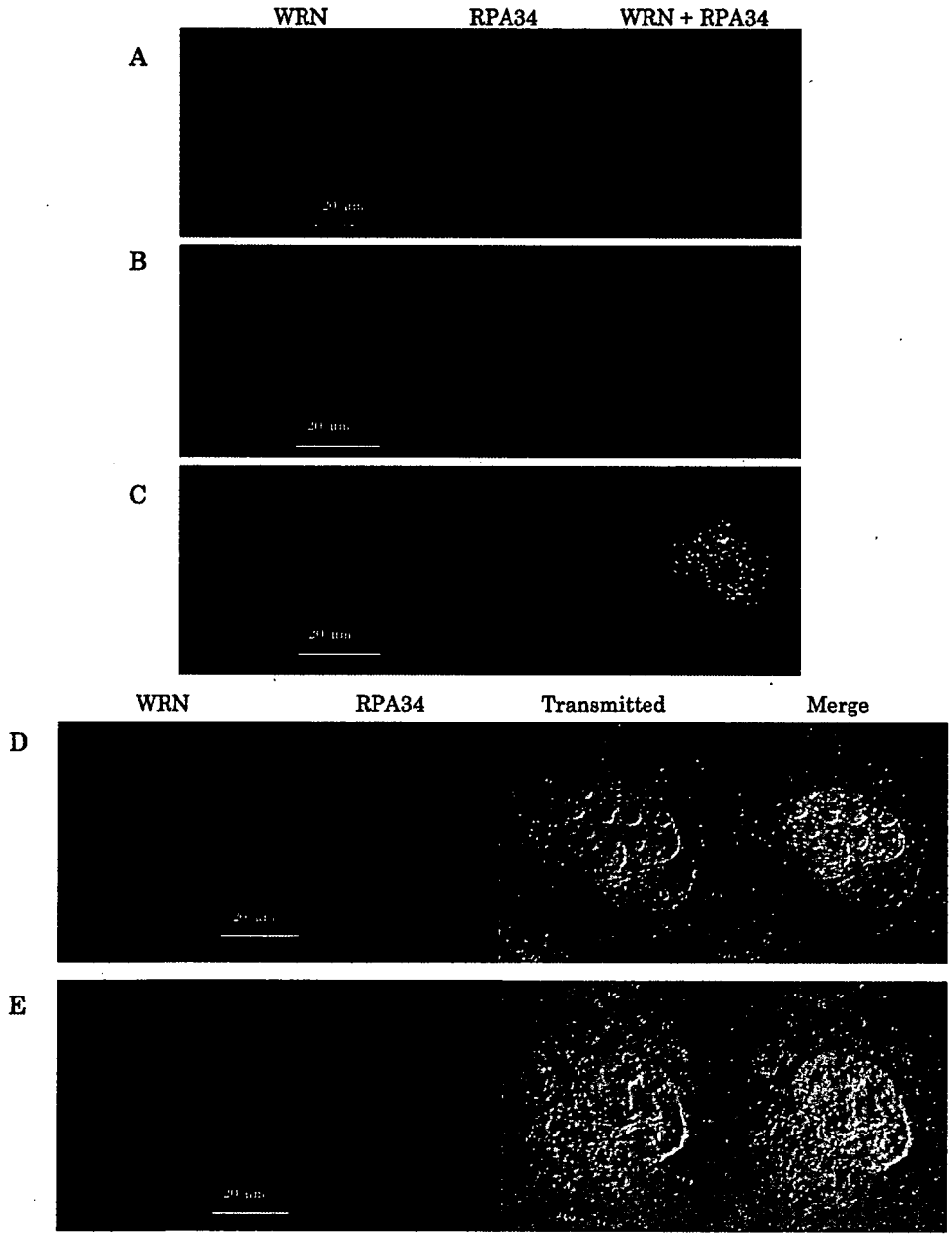

Fig. 3. Induction and Recovery of DNA Damage by CPT in HeLa Cells Assessed by Immunofluorescence

(A) Most of WRN was found in the nucleolus while RPA34 was dispersed in the nucleoplasm in the absence of CPT. (B) Down-regulation of WRN made some fraction of RPA34 form nuclear foci in the nucleoplasm. (C) DNA damage was induced by adding 10 nM of CPT during 6 h in HeLa cells. The nuclear foci at DNA-damaged sites stained with anti-WRN and anti-RPA34 antibodies were obvious and were co-localized. (D, E) At 30 h after transfection with *WRN*-siRNA or *NS*-siRNA, cells were cultured in the presence of 10 nM of CPT for 6 h. Then, the cells were further cultured for 3 h in the absence of CPT to recover DNA damage.

clear foci stained by both anti-WRN and RPA34 antibodies appeared in the nucleoplasm, as we previously reported.[17] The same staining profiles were also obtained with HeLa cells transfected with *NS*-siRNA used as negative control (Fig. 3C). Further culture of these cells in the CPT-free medium for 6 h causes most WRN proteins in the nuclear foci to return to the nucleolus leaving fewer numbers and smaller sizes of RPA34 foci on the nucleoplasmic DNA, suggesting that DNA repair was accomplished and that most nuclear foci consisting of WRN and RPA34 disappeared (Fig. 3D).

Under the same conditions, except the *NS*-siRNA was replaced by *WRN*-siRNA, CPT treated HeLa cells maintained many and significantly large RPA34 foci in the nucleoplasm even after removal of CPT at more than 6 h, suggesting that DNA repair was not completed and that the single-strand region was left unrepaired in the RPA34-bound form (Fig. 3E). It should be noted that most nuclear foci were not stained with WRN antibody as expected from the WRN siRNA treatment, nor was WRN helicase found in the nucleolus because of the silencing of WRN helicase. The data clearly showed that silencing WRN prevented repair of CPT-mediated DNA damages in the CPT-treated HeLa cells, and permitted the accumulation of DNA damage that explained the increased cytotoxicity of CPT in the combined treatment of CPT and *WRN*-siRNA. Similar effects were observed with cancer cell lines other than HeLa cells (data not shown). The data also explain why WS cells previously showed increased sensitivity to genotoxic reagents, including CPT.

The enzymatic activity of WRN to unwind long duplex DNA substrates is stimulated by RPA,[18] and WRN directly interacts with RPA as verified by co-immunoprecipitation of purified proteins.[19] WRN forms nuclear foci in response to genotoxins, including CPT, etoposide, 4NQO and bleomycin.[17] These WRN foci overlap with RPA foci almost entirely and with the foci of Rad51 partially, suggesting cooperative functions of these proteins in response to DNA damage.

The results of this study obtained by using *WRN*-siRNA at cellular levels were consistent with the following clinical results to treat colorectal cancer patients by using the CPT analogue Irinotecan, commonly used in the clinical setting to treat this tumor type.[20] The WRN function was eliminated in some of the human cancer cells by transcriptional silencing associated with CpG island-promoter hypermethylation. Importantly, *WRN* gene hypermethylation in colorectal tumors is a predictor of good clinical response to Irinotecan, due to the reduced WRN expression and increased CPT cytotoxicity. These findings highlighted the importance of *WRN* epigenetic inactivation in human cancer, leading to hypersensitivity to chemotherapeutic drugs.

WRN expression is augmented in rapidly growing cells, such as Epstein-Barr virus-infected and immortalized B limphoblastoid cells, much higher than in virus-infected and mortal B limphoblastoid cells.[21,22] Also, a wide variety of cancer cells show very high expressions of WRN in the same way as WRN in human fibroblast cells transfected with SV40 T antigen.[21] All these findings imply that many of cancer cells are perhaps "addicted to" (that is, physiologically dependent on) the specifically overexpressed WRN participating in DNA repair to maintain their rapid proliferation, analogously to the theory of cancer cell addiction to certain oncogenes proposed by Weinstein[23]; these kind of genes and gene products have been pursued as an ideal chemotherapeutic target for anti-cancer agents with few adverse effects.[24] In addition, administration of WRN-siRNA to cancer cells by an appropriate drug delivery system, such as positively charged liposome that are incorporated more efficiently in rapidly growing cancer cells than non-cancerous resting cells, should lower the cytotoxic dose of CPT preferentially in cancer cells, benefiting patients by fewer adverse effects in their normal tissues and cells.

REFERENCES AND NOTES

1) Present address: *Japan Biological Information Research Center (JBIRC), Japan Biological Informatics Consortium (JBIC); 2–42 Aomi, Koutou-ku, Tokyo 135–0064, Japan.*
2) Present address: *Department of Cellular and Molecular Biology, Hiroshima University; 1–2–3 Kasumi, Minami-ku, Hiroshima 734–8553, Japan.*
3) Goto M., Miller R. W. (eds.), "From Premature Gray Hair to Helicase—Werner Syndrome: Implications for Aging and Cancer," Japan Scientific Societies Press & Karger, Tokyo, 2001.
4) Yu C. E., Oshima J., Fu Y. H., Wijsman E. M., Hisama F., Alisch R., Matthews S., Nakura J., Miki T., Ouais S., Martin G. M., Mulligan J., Schellenberg G. D., *Science*, **272**, 258—262 (1996).
5) Shimamoto A., Sugimoto M., Furuichi Y., *Int. J. Clin. Oncol.*, **9**, 288—298 (2004).
6) Sharma A., Awasthi S., Harrod C. K., Matlock E. F., Khan S., Xu L., Chan S., Yang H., Thammavaram C. K., Rasor R. A., Burns D. K., Skiest D. J., Van Lint C., Girard A.-M., McGee M., Monnat R. J., Jr., Harrod R., *J. Biol. Chem.*, **282**, 12048—12057 (2007).
7) Matsumoto T., Shimamoto A., Goto M., Furuichi Y., *Nature Genet.*, **16**, 335—336 (1997).
8) Gebhart E., Bauer R., Raub U., Schinzel M., Ruprecht K. W., Jonas J. B., *Hum. Genet.*, **80**, 135—139 (1988).
9) Ogburn C. E., Oshima J., Poot M., Chen R., Hunt K. E., Gollahon K. A., Rabinovitch P. S., Martin G. M., *Hum. Genet.*, **101**, 121—125 (1997).
10) Okada M., Goto M., Furuichi Y., Sugimoto M., *Biol. Pharm. Bull.*, **21**, 235—239 (1998).
11) Poot M., Gollahon K. A., Rabinovitch P. S., *Hum. Genet.*, **104**, 10—14 (1999).
12) Lebel M., Leder P., *Proc. Natl. Acad. Sci. U.S.A.*, **95**, 13097—13102 (1998).
13) Elbashir S. M., Harborth J., Lendeckel W., Yalcin A., Weber K., Tuschl T., *Nature* (London), **411**, 494—498 (2001).
14) Shiratori M., Sakamoto S., Suzuki N., Tokutake Y., Kawabe Y., Enomoto T., Sugimoto M., Goto M., Matsumoto T., Furuichi, Y., *J. Cell Biol.*, **144**, 1—9 (1999).
15) Mosmann T., *J. Immunol. Methods*, **65**, 55—63 (1983).
16) Marciniak P. A., Lombard D. B., Johnson F. B., Guarente L., *Proc. Natl. Acad. Sci. U.S.A.*, **95**, 6887—6892 (1998)
17) Sakamoto S., Nishikawa K., Heo S. J., Goto M., Furuichi Y., Shimamoto A., *Genes Cells*, **6**, 421—430 (2001).
18) Shen J. C., Gray M. D., Oshima J., Kamath-Loeb A. S., Fry M., Loeb L. A., *J. Biol. Chem.*, **273**, 34139—34144 (1998).
19) Brosh R. M., Jr., Orren D. K., Nehlin J. O., Ravn P. H., Kenny M. K., Machwe A., Bohr V. A., *J. Biol. Chem.*, **274**, 18341—18350 (1999).
20) Agrelo R., Cheng W. H., Setien F., Ropero S., Espada J., Fraga M. F., Herranz M., Paz M. F., Sanchez-Cespedes M., Artiga M. J., Guerrero D., Castells A., von Kobbe C., Bohr V. A., Esteller M., *Proc. Natl. Acad. Sci. U.S.A.*, **103**, 8822—8827 (2006).
21) Kawabe T., Tsuyama N., Kitao S., Nishikawa K., Shimamoto A., Shiratori M., Matsumoto T., Anno K., Sato T., Mitsui Y., Seki M., Enomoto T., Goto M., Ellis N. A., Ide T., Furuichi Y., Sugimoto M., *Oncogene*, **19**, 4764—4772 (2000).
22) Sugimoto M., Furuichi Y., Ide T., Goto M., *J. Virol.*, **73**, 9690—9691 (1999).
23) Weinstein I. B., *Science*, **297**, 63—64 (2002).
24) Sharma S. V., Gajowniczek P., Way I. P., Lee D. Y., Jiang J., Yuza Y., Classon M., Haber D. A., Settleman J., *Cancer Cell*, **10**, 425—435 (2006).